Taxvig C, Viggaard AM, Hass U, Axelstad M, Boberg J, Hansen PR, et al. Do parabens have the ability to interfere with steroidogenesis. Toxicol Sci 2008;106:206–13.

Tay TW, Andriana BB, Ishii M, Choi EK, Zhu XB, Alam MS, et al. Phagocytosis plays an important role in clearing dead cells caused by mono(2-ethylhexyl) phthalate administration. Tissue Cell 2007;39:241–6.

Tesarik J, Greco E, Cohen-Bacrie P, Mendoza C. Germ cell apoptosis in men with complete and incomplete spermiogenesis failure. Mol Hum Reprod 1998;4:757–62.

vom Saal FS, Cooke P, Buchaman DL, Palanza PP, Thayer KA, Nagel SC, et al. A physiologically based approach to the study of bisphenol A and other estrogenic chemicals on the size of reproductive organs, daily sperm production, and behaviour. Toxicol Ind Health 1998;14:239–60.

Yan W, Suominen J, Samson M, Jegou B, Toppari J. Involvement of Bcl-2 family proteins in germ cell apoptosis during testicular development in the rat and pro-survival effect of stem cell-factor on germ cells in vitro. Mol Cell Endocrinol 2000;165:115–29.

Toxicology Letters 228 (2014) 235–240

Contents lists available at ScienceDirect

Toxicology Letters

journal homepage: www.elsevier.com/locate/toxlet

Peroxisome proliferator-activated receptor α mediates di-(2-ethylhexyl) phthalate transgenerational repression of ovarian *Esr1* expression in female mice

Michihiro Kawano[a,b,1], Xian-Yang Qin[a,1], Midori Yoshida[c], Tomokazu Fukuda[d], Hiroko Nansai[a], Yumi Hayashi[e], Tamie Nakajima[f], Hideko Sone[a,*]

[a] Research Center for Environmental Risk, National Institute for Environmental Studies, Tsukuba, Ibaraki, Japan
[b] Department of Nursing, School of Health Sciences, Ibaraki Prefectural University of Health Science, Inashiki-gun, Ibaraki, Japan
[c] Division of Pathology, Biological Safety Research Center, National Institute of Health Sciences, Setagaya-ku, Tokyo, Japan
[d] Department of Animal Production Science, Graduate School of Agricultural Science, Tohoku University, Sendai, Miyagi, Japan
[e] Pathophysiological Laboratory Sciences, Department of Radiological and Medical Laboratory Sciences, Nagoya University Graduate School of Medicine, Nagoya, Aichi, Japan
[f] College of Life and Health Sciences, Chubu University, Kasugai, Aichi, Japan

HIGHLIGHTS

- Effect of DEHP on ovarian gene expression is measured in PPARα knockout mice.
- Transgenerational repression of ovarian Esr1 expression by DEHP is found in WT mice.
- DEHP regulation of ovarian Esr1 gene expression is lost in PPARα-knockout mice.
- Transgenerational effect of DEHP is partly mediated by PPARα-dependent pathways.

ARTICLE INFO

Article history:
Received 19 October 2013
Received in revised form 20 April 2014
Accepted 23 April 2014
Available online 5 May 2014

Keywords:
DEHP
PPARα
Transgenerational
Female mice
Reproductive

ABSTRACT

Di-(2-ethylhexyl)-phthalate (DEHP) is a phthalate ester that binds peroxisome proliferator-activated receptor α (PPARα) to induce proliferation of peroxisomes and regulate the expression of specific target genes. The question of whether the effect of DEHP on female reproductive processes is mediated via PPARα-dependent signaling is controversial. In this study, we investigated the effect of exposure to DEHP on ovarian expression of estrogen receptor α (*Esr1*) and aromatase (*Cyp19a1*) in three generations of Sv/129 wild-type (WT, +/+) and PPARα (−/−) knockout mice. Compared with untreated controls, ovarian expression of *Esr1* decreased in response to DEHP treatment in the F0 (0.56-fold, $P=0.19$), F1 (0.45-fold, $P=0.023$), and F2 (0.35-fold, $P=0.014$) generations of WT mice, but not PPARα-null mice. Our data indicate that transgenerational repression by DEHP of ovarian *Esr1* gene expression is mediated by PPARα-dependent pathways. Further studies are required to elucidate the mechanisms underlying crosstalk between PPARα and Esr1 signaling in reproductive processes.

1. Introduction

Because of their common industrial application as plasticizers, phthalates esters are highly prevalent in the environment (Halden, 2010). Di-(2-ethylhexyl)-phthalate (DEHP), which is commonly used as a plasticizer of polyvinyl chloride (PVC), has been characterized as an endocrine disruptor on the basis of its anti-androgen activity (Fisher, 2004). Given its ability to cross the placenta and pass into breast milk, considerable concern has been raised over the potential harm to the developing fetus and newborn arising from exposure to DEHP (Adibi et al., 2008). Several well-designed epidemiological studies have consistently documented the anti-androgenic effects of prenatal exposure to DEHP on indices of male reproductive development, such as decreased anogenital index (AGI) in male neonates (Suzuki et al., 2012; Swan, 2008; Swan et al., 2005). Occupational exposure to DEHP also showed positive associations with sperm DNA denaturation induction and negative

* Corresponding author. Tel.: +81 29 850 2464; fax: +81 29 850 2546.
E-mail address: hsone@nies.go.jp (H. Sone).
[1] These authors contributed equally.

http://dx.doi.org/10.1016/j.toxlet.2014.04.019
0378-4274/

associations with sperm motility (Huang et al., 2011). However, no significant relationships between prenatal exposure to DEHP and birth outcomes were also reported (Suzuki et al., 2010). Although there has been a controversy about its toxicity, many scientific and professional organizations have made recommendations to reduce DEHP exposure in pregnant women and young children to prevent unexpected consequences of reproductive and development effects in the offspring (Braun et al., 2013).

In rodents, it has become apparent that DEHP exposure might affect the development of reproductive tract by decreasing fetal testosterone synthesis during sexual differentiation in male rats and mice (Wolf et al., 1999; Wu et al., 2012; Zacharewski et al., 1998). Exposure to DEHP *in utero* and during lactation at dose levels relevant to humans also causes a significant delay in indices of pubertal onset in female offspring rats, such as vaginal opening (Miller and Auchus, 2011). Moreover, long-term DEHP exposure has been associated with reduced serum levels of estradiol, follicle-stimulating hormone (FSH), pituitary FSH and luteinizing hormone in female rats (Andrade et al., 2006). Despite these studies, comprehensive information on the molecular mechanism underlying the potential endocrine disruptive effect of low-dose DEHP exposure on reproductive function in female animal model is lacking.

Peroxisome proliferator-activated receptor α (PPARα), a ligand-regulated member of the nuclear receptor superfamily of transcription factors, was the first of three members of the PPAR family identified in the 1990s (Arcadi et al., 1998). By modulating the expression of peroxisomal lipid metabolism and growth regulatory genes, activation of PPARs plays an important role in the metabolism of xenobiotics (Lovekamp-Swan and Davis, 2003). Consistent with weak PPARα agonism of DEHP (Haynes-Johnson et al., 1999), we have previously shown that hepatic PPARα is required for the toxic effect of maternal exposure to DEHP in male offspring mice (Hayashi et al., 2011). Moreover, PPARα transcript is also related to the effect of DEHP on metabolism and fertility in female mice (Schmidt et al., 2012). On the other hand, recent evidences also indicated that DEHP can induce liver tumorigenesis through a PPARα-independent pathway (Ito et al., 2007). These studies aside however, the role of PPARα in the developmental and reproductive toxicity associated with DEHP exposure is unclear (Kobayashi et al., 2009). Accordingly, to clarify the potential role of PPARα in the effects of DEHP on female reproductive health, we compared the transgenerational effect of DEHP on ovarian gene expression in wild-type (WT, +/+) and PPARα (−/−) knockout mice.

2. Materials and methods

2.1. Experimental animals

Experiments in this study were conducted according to the Guidelines for Animal Experiments of Shinshu University, Japan. WT and PPARα knockout mice in the Sv/129 genetic background were generated as described elsewhere (Lee et al., 1995). Animal husbandry was performed in a clean room with controlled temperature, relative humidity, and light with 12-h light/dark cycle, as previously described (Hayashi et al., 2011).

2.2. DEHP exposure

DEHP (CAS No. 117-82-7) was purchased from Wako Pure Chemistries (Osaka, Japan). Corn oil (Sigma Chemical Company, St. Louis, MO, USA) was used as the vehicle control. Mating was set up according to the schedule previously described (Hayashi et al., 2011). WT and PPARα knockout mice were given a diet containing vehicle control or 0.05% DEHP (approximately 80 mg/kg/day) through three generations ($n = 6$ in each group in each generation). DEHP was administered starting in the F0 generation at 12 weeks of age and continuing to the end of experiment in the F2 generation. Mice were sacrificed by CO_2 asphyxiation at 36 weeks of age in the F0 generation and at 16 weeks of age in the F1 and F2 generations (Fig. 1). Blood samples were taken from the abdominal aorta and plasma was separated by centrifugation at 4 °C and stored at 80 °C until assay for testosterone and estradiol. Body and organs such as liver and ovaries were dissected out and weighed as quickly as possible. Then ovarian tissue samples for RNA analysis were separated into two sections, one of which was snap-frozen in liquid nitrogen and stored at −80 °C, while the other was fixed in buffered formalin for 6–24 h. Concentrations of testosterone and estradiol in plasma were measured by a testosterone or estradiol EIA kit (Cayman, Ann Arbor, MI).

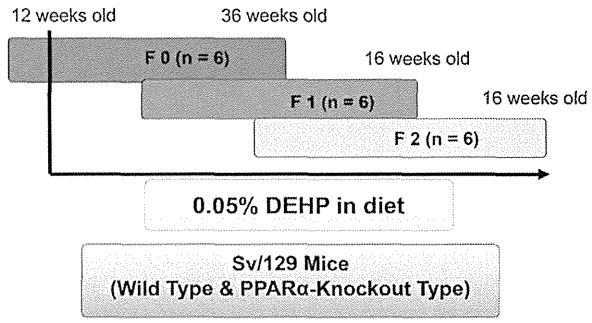

Fig. 1. Schedule of transgenerational exposure to dietary DEHP. Maternal mice of both genotypes in the F0 generation were exposed to DEHP in their diet from 16 to 36 weeks of age. Offspring (F1) and third-generation (F2) mice were also exposed to dietary DEHP until 16 weeks of age.

2.3. Quantitative real-time reverse transcription-polymerase chain reaction (RT-PCR)

Total RNA was isolated from a frozen ovary using an ISOGEN kit from NIPPON GENE (Tokyo, Japan) following instructions from the manufacturer. Quantification and quality assessment of the isolated RNA samples were performed and verified using an Agilent Bioanalyzer 2100 and an RNA 6000 Nano Assay (Agilent Technologies, Palo Alto, CA, USA) in accordance with the manufacturer's instructions. cDNA was synthesized using random primers (Perkin-Elmer Applied Biosystems Inc., Tokyo, Japan). Oligonucleotide primers and TaqMan probe were designed using Primer Express, version 1.0 (Applied Biosystems, Foster City, CA, USA) and Oligo 5.1 software (National Bioscience, Plymouth, MN, USA) based on GenBank database sequences as follows: *Esr1* (Accession # M38651), primer sequences 5′-tcaactgggcaaagagagtg-3′ and 5′-gtgctggacagaaacgtgta-3′ TaqMan probe sequences 5′-agtgtgcctggctggagattctgatgatt-3′; *Cyp19a1* (aromatase) (Accession # D00659), primer sequences 5′-gaaagagaacgtgaatcagtg-3′ and 5′-atgatgttagttccctttttta-3′, TaqMan probe sequences 5′-ttaatgaaagcatgcggtaccagcct-3′; *Gapdh* (Accession# M32599), primer sequences 5′-tgcagtggcaaagtggagatt-3′ and 5′-gttgaatttgccgtgagtggag-3′ TaqMan probe sequences 5′-ccatcaacgacccctt-3′. The amplification reaction was performed in an ABI PRISM 7000 Sequence Detector (Applied Biosystems) under the following cycling conditions: 95 °C for 10 min, followed by 50 cycles of 95 °C for 15 s, 56 °C for 1 min and 72 °C for 30 s. The gene expression levels were calculated based on the threshold cycle using Sequence Detection System Software (Applied Biosystems). Gene expression was normalized according to *Gapdh* expression levels.

2.4. Histological analysis

Ovarian tissue samples fixed in 10% neutral buffered formalin were embedded in paraffin and sliced into 5-μm sections. Three sections on the cut surface of the maximum width diameter of ovary per animal were observed. The number of follicles in one slice out of three was counted. Ovarian tissue sections were stained with hematoxylin and eosin and the number and size of follicle and corpus luteum were examined under a light microscope using an Olympus BX50 (Olympus, Tokyo, Japan).

2.5. Bioinformatics and statistical analysis

Quantitative data were expressed as the mean ± standard deviation. For body and organs weight, hormone concentrations, multiple comparisons were made between the exposure groups and the control group using Dunnett's test after one-way ANOVA. Statistical analysis was performed by the two-tailed Student's *t*-test. Relationships were considered statistically significant at $P < 0.05$. Molecular network underlying the reproductive effect of DEHP was analyzed using the Ingenuity Pathway Analysis program (Ingenuity Systems, Mountain View, CA, USA).

3. Results

3.1. Transgenerational effect of DEHP exposure on body, liver, ovary weights, and sex hormones in WT and PPARα knockout mice

No abnormalities were apparent during clinical observation in any generation of WT and PPARα knockout DEHP-treated mice

Table 1
Generational comparison of body, liver, ovary weights, and sex hormones in female WT and PPARα knockout mice[a].

Generation	F0 control	F0 DEHP	F1 control	F1 DEHP
WT				
Number of mice	6	6	6	6
Body weight	28.0 ± 3.7	30.2 ± 1.3	26.7 ± 1.3	22.7 ± 2.2
Liver weight	0.87 ± 0.07	1.04 ± 0.11	0.93 ± 0.04	0.73 ± 0.09
Liver/body (%)	3.12 ± 0.14	3.46 ± 0.24	3.49 ± 0.01	3.19 ± 0.14
Ovary weight	0.014 ± 0.0001	0.014 ± 0.0000	0.015 ± 0.0020	0.014 ± 0.0010
Ovary/body (%)	0.048 ± 0.007	0.047 ± 0.003	0.054 ± 0.004	0.061 ± 0.006
Testosterone (ng/mL)	0.20 ± 0.08	0.45 ± 0.07	0.10 ± 0.05	0.22 ± 0.06
Estradiol (pg/mL)	27 ± 5	49 ± 18	22 ± 5	38 ± 11
PPARα-knockout				
Number of mice	6	6	6	6
Body weight	26.0 ± 1.6	31.8 ± 2.6	21.0 ± 0.9	23.4 ± 3.7
Liver weight	0.94 ± 0.21	1.51 ± 0.17	0.71 ± 0.05	0.71 ± 0.10
Liver/body (%)	3.60 ± 0.58	4.75 ± 0.52	3.40 ± 0.34	3.05 ± 0.17
Ovary weight	0.015 ± 0.004	0.017 ± 0.003	0.013 ± 0.004	0.015 ± 0.0020
Ovary/body (%)	0.059 ± 0.010	0.055 ± 0.008	0.061 ± 0.018	0.063 ± 0.010
Testosterone (ng/mL)	0.15 ± 0.07	0.23 ± 0.06	0.10 ± 0.04	0.20 ± 0.14
Estradiol (pg/mL)	26 ± 11	26 ± 4	21 ± 6	28 ± 4

[a] Mean ± standard deviation. Significant differences from control for all data except the sex hormones were performed by the Dunnett's test.
[b] Number of animals for testosterone and estradiol data were two to four in each group.

prior to sacrifice and necropsy. Similarly, DEHP treatment had no significant effect on body, liver, and ovary weight in female dams (F0) and offspring (F1) in either WT or PPARα knockout mice. Of interest, increase of circulating estradiol was observed only in WT but not PPARα knockout mice (Table 1).

3.2. Effect of DEHP on ovarian Esr1 expression in WT and PPARα knockout mice

We next examined the effect of DEHP exposure on ovarian *Esr1* gene expression in WT and PPARα knockout mice (Fig. 2). Compared with controls, ovarian *Esr1* expression decreased in response to dietary 0.05% DEHP in the F0 (0.56-fold, $P = 0.19$), F1 (0.45-fold, $P = 0.023$), and F2 (0.35-fold, $P = 0.014$) generations of WT mice. In contrast, DEHP had no significant on ovarian *Esr1* gene expression in either the F0 (1.49-fold, $P = 0.18$), F1 (1.00-fold, $P = 0.49$), or F2 (0.80-fold, $P = 0.27$) generations of PPARα knockout mice.

3.3. Effect of DEHP on the ovarian Cyp19a1 (aromatase) gene expression in F2 mice

Next, we compared the effect of DEHP exposure on ovarian *Cyp19a1* (aromatase) gene expression in WT and PPARα knockout F0 dams (Fig. S1) and the F2 generation (Fig. 3). We observed no statistically significant changes of ovarian *Cyp19a1* expression in response to DEHP treatment in both WT and PPARα knockout mice.

Supplementary figure related to this article can be found, in the online version, at http://dx.doi.org/10.1016/j.toxlet.2014.04.019.

3.4. Histopathological examination of ovaries of F2 mice exposed to DEHP

Histopathological analysis of uteri and ovaries from F0, F1, and F2 WT and PPARα knockout mice treated with control diet or 0.05%

Table 2
Histopathological findings in F0, F1, and F2 female WT and PPARα knockout mice.

Generation & PPARα genotype treatment group	No of mice	Ovary							Uterus						
		Corpus luteum			Follicles				Similar histology to cycle						
		Total	New	Old	Graafian	Medium	Small	Atresia	P	E	M	M/D	D	D/P	Others
F0 WT															
Control	3	2.3 ± 2.1	2.3 ± 2.1	0	−/+	−/+	+/++	+/++	1		2				
DEHP	4	2.8 ± 2.4	1.8 ± 2.0	1 ± 0.7	−/+	−/++	+/++	+/++	2				2		
F0 PPARα-knockout															
Control	3	2.3 ± 0.9	2 ± 0.8	0.3 ± 0.5	−/+	−/++	+/++	+/++			1	1		1	
DEHP	4	4.0 ± 3.1	NE1	NE1	−/+	−/++	+/++	−/+/++		1	2			1	
F1 WT															
Control	3	3.7 ± 1.2	3.7 ± 1.2	0	−/+	+	+/++	+/++	1		1		1		
DEHP	7	2.9 ± 1.5	2.6 ± 1.2	0.3 ± 0.7	−/+	−/+	+/++	++	1	2	3		1		
F1 PPARα-knockout															
Control	3	10 ± 0.8	0.3 ± 0.5	0.7 ± 0.9	−/+	+	++	+/++	1		1	1			
DEHP	5	1.4 ± 0.8	1.4 ± 0.8	0	−/+	−/+	+/++	+/++	2	1		1		1	
F2 WT															
Control	5	43 ± 0.8	NE1	NE1	−	+/++	+	+	NE2						
DEHP	5	1.8 ± 0.4	NE1	NE1	−	+/++	+/++	+/++	NE2						
F2 PPARα-knockout									NE2						
Control	5	3.2 ± 0.8	NE1	NE1	−	+	+	+/++	NE2						
DEHP	5	2.0 ± 1.1	NE1	NE1	−	+/++	+	+/++	NE2						

NE1: not available for detailed classification; NE2, not examined. Similar morphology in the uterus to those at P, proestrus; E, estrus; M, metestrus; D, diestrus.

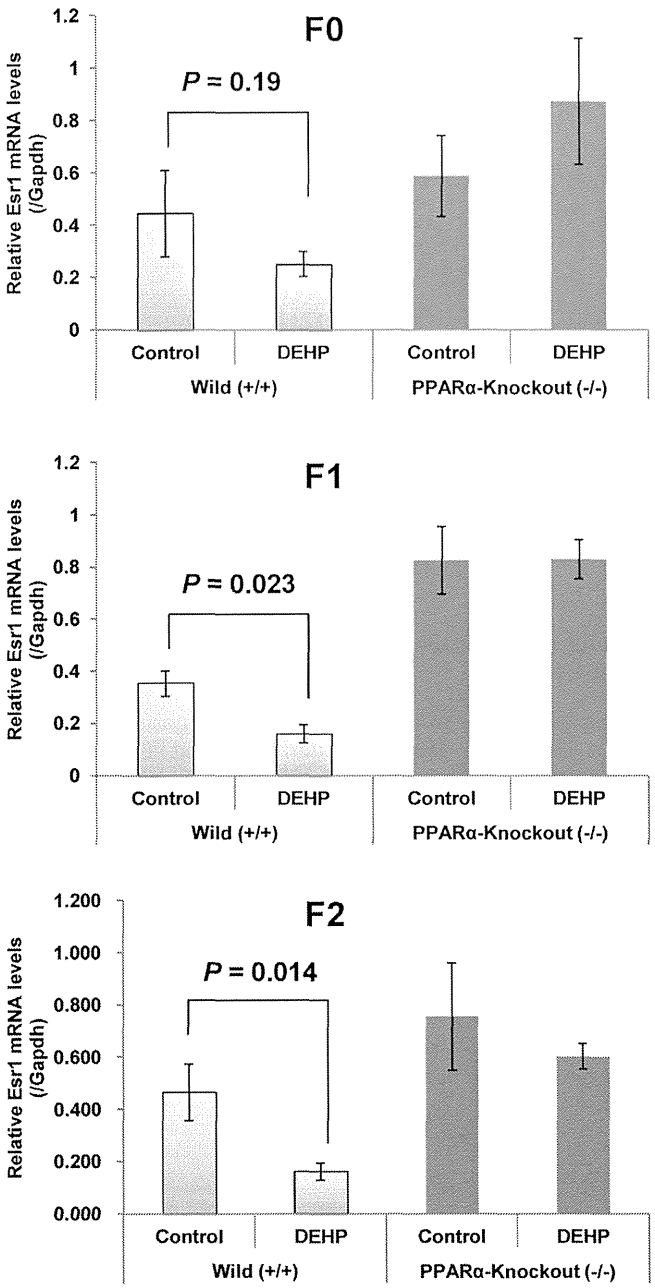

Fig. 2. Effect of DEHP on ovarian *Esr1* gene expression in WT and PPARα knockout mice. Gene expression levels were normalized to GAPDH and values are reported as mean ± standard deviation.

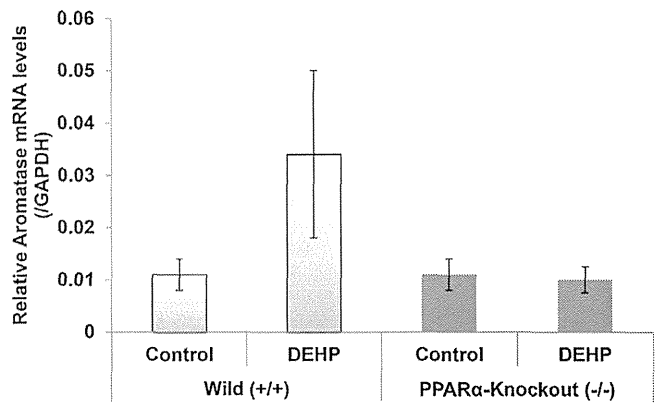

Fig. 3. Effect of DEHP on ovarian aromatase gene expression in WT and PPARα knockout mice. Gene expression levels were normalized to GAPDH and values are reported as mean ± standard deviation.

DEHP diet is shown in Fig. 4 and quantitative data are summarized in Table 2. Although ovary size varied, with those in the F1 generation of control diet-PPARα knockout mice being notably small, most ovaries had corpora lutea and growing follicles, indicating that ovulation and estrous cycle were unaffected by DEHP treatment. Moreover, no morphological differences were observed among genotypes and DEHP treatment. Histopathological examination indicated that DEHP exposure had no significant effect on the number of primary ovarian follicles in either WT or PPARα knockout mice.

4. Discussion

Plastics have become indispensable in modern society, with annual global production exceeding 300 million tons (Halden, 2010). DEHP is the most commonly used phthalate plasticizer for PVC and has been described as an endocrine disruptor for its anti-androgen activity (Fisher, 2004). The public health threat posed by phthalate-tainted foodstuffs is exemplified in Taiwan, where elevated concentrations (~2108 ppm) of DEHP have been detected in a wide variety of food products, including sports drinks, fruit beverages, tea drinks, fruit jam/nectar/jelly, and health food supplements (Wu et al., 2012). To determine the effect of DEHP on female reproductive health, and to clarify the molecular basis of this effect, we set out here to study the transgenerational effect of DEHP on ovarian gene expression in Sv/129 WT and PPARα knockout mice. We found that ovarian *Esr1* expression was reduced in response to DEHP treatment in the F0, F1, and F2 generations of WT mice but not in PPARα-knockout mice, indicating that the adverse transgenerational effects of DEHP on female reproductive health are mediated at least in part by PPARα.

It has been hypothesized that DEHP is an estrogenic endocrine disruptor *in vivo* but not *in vitro* (Wolf et al., 1999; Zacharewski et al., 1998). Consistent with such a notion, we previously found no estrogenic effect of DEHP in Esr1-positive BG1Luc4E2 human

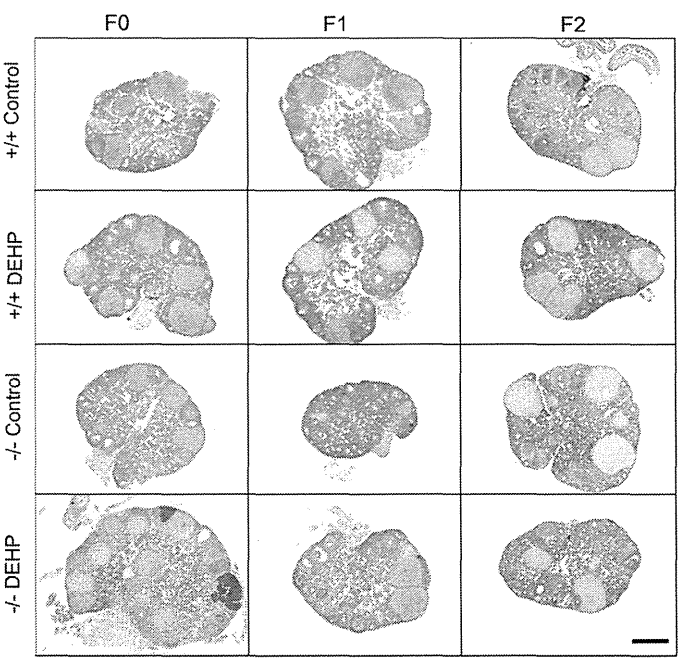

Fig. 4. Ovaries of three generations of WT and PPARα knockout mice in the control and DEHP-treated groups. Scale bar: 50 μm.

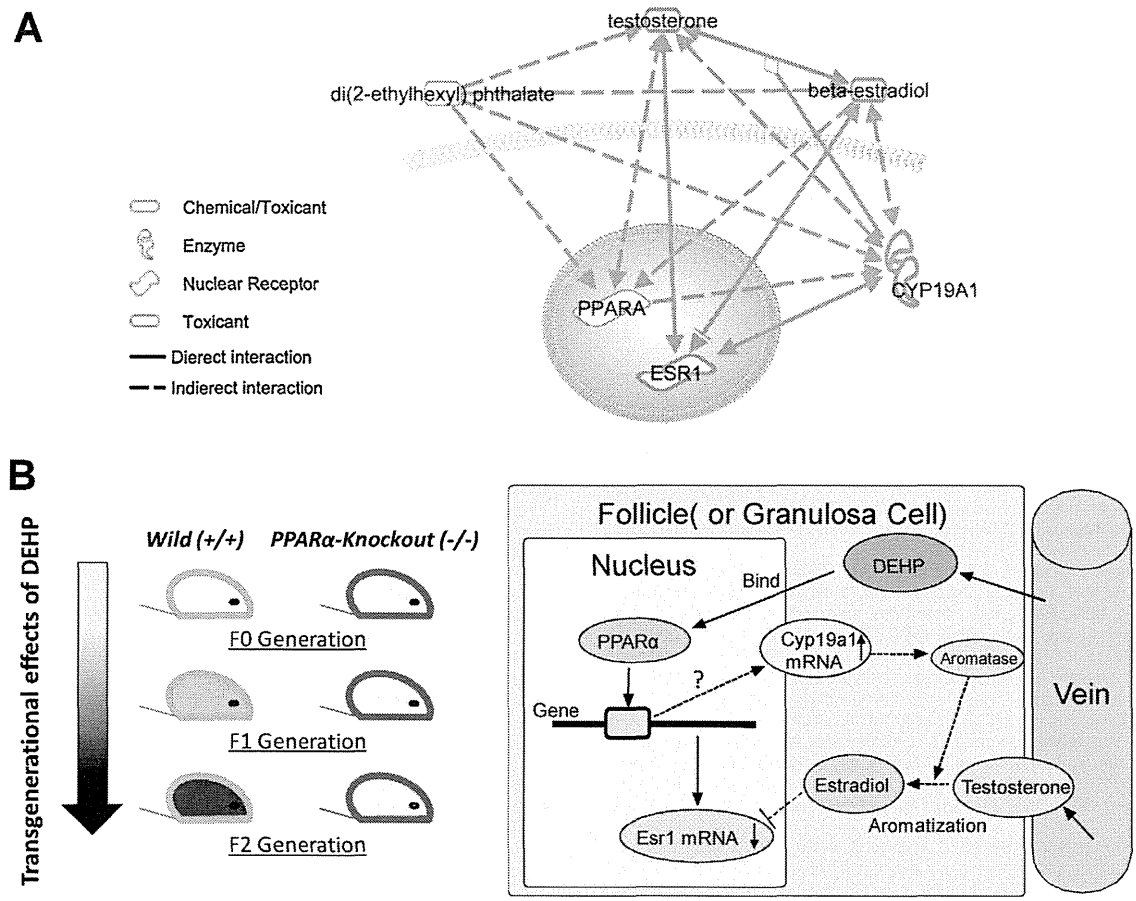

Fig. 5. Schematic diagram of molecular mechanism involved in the reproductive effect of DEHP. (A) The knowledge-based network generated by IPA. (B) Schematic model showing the potential PPARα-dependent pathways of the transgenerational adverse reproductive effects of DEHP in female mice.

ovarian cancer cells at concentrations as high as 0.1 mM (Qin et al., 2011). In contrast, in this present *in vivo* study, increased serum estradiol contents and reduced ovarian *Esr1* gene expression were observed in WT mice fed with 0.05% DEHP (Table 1 and Fig. 2). Aromatase (Cyp19a1) catalyzes the conversion of androstenedione to estrone and testosterone to estradiol (Miller and Auchus, 2011), which are key steps in estrogen biosynthesis. Non-monotonic dose–response effects of DEHP exposure on aromatase activity have been reported in male rats, such that low doses are inhibitory and high doses are stimulatory (Andrade et al., 2006), and it has been suggested that the endocrine-disrupting effect of DEHP development of the male reproductive tract is related to inhibition of testosterone (Arcadi et al., 1998). Production of estradiol, which plays an essential role in female reproductive physiology, is mediated by FSH signaling, which stimulates aromatase activity in ovarian granulosa cells to induce the synthesis of estradiol from testosterone (Haynes-Johnson et al., 1999). Excess estradiol in the ovary has been suggested to inhibit ovarian *Esr1* expression because of the negative feedback regulation of the interaction between Esr1 and its ligand (Kobayashi et al., 2009). According to the IPA knowledgebase, which is an extensive database of functional interactions that are drawn from peer-reviewed publications (Calvano et al., 2005), it is assumed that DEHP activates PPARα to increase ovarian aromatase expression, which in turn promotes the synthesis of estradiol from testosterone. Elevated levels of estradiol subsequently inhibit *Esr1* expression via negative feedback of the Esr1-ligand interaction (Fig. 5). However, as the induction of ovarian aromatase by DEHP observed in our study failed to reach statistical significance, further study is needed to understand the role of aromatase in DEHP-induced adverse reproductive effect.

The PPARα dependence of the effect of DEHP on female reproductive health is a subject of controversy (Kobayashi et al., 2009). For example, while we previously showed that hepatic PPARα is required for the toxic effect of maternal exposure to DEHP in male offspring of mice (Hayashi et al., 2011), DEHP has also been shown to induce liver tumorigenesis via a PPARα-independent pathway (Ito et al., 2007). In the present study, we found that DEHP regulation of ovarian *Esr1* gene expression in WT mice was lost in PPARα-knockout mice, indicating that the transgenerational regulation of ovarian gene expression by DEHP is at least partly PPARα dependent. Consistent with this observation, a recent study showed that reductions in the number of methylated CpG sites of imprinted genes in the oocytes of F1-treated mice oocytes are transferable to F2 offspring, suggesting that DEHP has an epigenetic effect in oocytes (Li et al., 2014).

In summary, our data indicate that transgenerational repression by DEHP of ovarian *Esr1* gene expression is mediated by PPARα-dependent pathways. The possible mechanism might relate with negative feedback of the Esr1-ligand interaction (Fig. 5). Further studies are required to elucidate the crosstalk between PPARα and Esr1 signaling in reproductive processes.

Conflict of interest

The authors declare that there are no conflicts of interest.

Transparency document

The Transparency document associated with this article can be found in the online version.

Acknowledgments

This study was partly supported by the Environmental Rechnology Development Fund (ERTDF R01 H19-21) to H.S. that was granted by the Ministry of Environment, Japan. The funding agency had no role in the study design, data collection and analysis, decision to publish, or preparation of the manuscript.

References

Adibi, J.J., Whyatt, R.M., Williams, P.L., Calafat, A.M., Camann, D., Herrick, R., Nelson, H., Bhat, H.K., Perera, F.P., Silva, M.J., Hauser, R., 2008. Characterization of phthalate exposure among pregnant women assessed by repeat air and urine samples. Environ. Health Perspect. 116, 467–473.

Andrade, A.J., Grande, S.W., Talsness, C.E., Grote, K., Chahoud, I., 2006. A dose–response study following in utero and lactational exposure to di-(2-ethylhexyl)-phthalate (DEHP): non-monotonic dose–response and low dose effects on rat brain aromatase activity. Toxicology 227, 185–192.

Arcadi, F.A., Costa, C., Imperatore, C., Marchese, A., Rapisarda, A., Salemi, M., Trimarchi, G.R., Costa, G., 1998. Oral toxicity of bis(2-ethylhexyl) phthalate during pregnancy and suckling in the Long-Evans rat. Food Chem. Toxicol. 36, 963–970.

Braun, J.M., Sathyanarayana, S., Hauser, R., 2013. Phthalate exposure and children's health. Curr. Opin. Pediatr. 25, 247–254.

Calvano, S.E., Xiao, W., Richards, D.R., Felciano, R.M., Baker, H.V., Cho, R.J., Chen, R.O., Brownstein, B.H., Cobb, J.P., Tschoeke, S.K., Miller-Graziano, C., Moldawer, L.L., Mindrinos, M.N., Davis, R.W., Tompkins, R.G., Lowry, S.F., Inflamm, Host Response to Injury Large Scale Collab. Res, P., 2005. A network-based analysis of systemic inflammation in humans. Nature 437, 1032–1037.

Fisher, J.S., 2004. Environmental anti-androgens and male reproductive health: focus on phthalates and testicular dysgenesis syndrome. Reproduction 127, 305–315.

Halden, R.U., 2010. Plastics and health risks. Annu. Rev. Public Health 31, 179–194.

Hayashi, Y., Ito, Y., Yamagishi, N., Yanagiba, Y., Tamada, H., Wang, D., Ramdhan, D.H., Naito, H., Harada, Y., Kamijima, M., Gonzales, F.J., Nakajima, T., 2011. Hepatic peroxisome proliferator-activated receptor alpha may have an important role in the toxic effects of di(2-ethylhexyl)phthalate on offspring of mice. Toxicology 289, 1–10.

Haynes-Johnson, D., Lai, M.T., Campen, C., Palmer, S., 1999. Diverse effects of tyrosine kinase inhibitors on follicle-stimulating hormone-stimulated estradiol and progesterone production from rat granulosa cells in serum-containing medium and serum-free medium containing epidermal growth factor. Biol. Reprod. 61, 147–153.

Huang, L.P., Lee, C.C., Hsu, P.C., Shih, T.S., 2011. The association between semen quality in workers and the concentration of di(2-ethylhexyl) phthalate in polyvinyl chloride pellet plant air. Fertil. Steril. 96, 90–94.

Ito, Y., Yamanoshita, O., Asaeda, N., Tagawa, Y., Lee, C.H., Aoyama, T., Ichihara, G., Furuhashi, K., Kamijima, M., Gonzalez, F.J., Nakajima, T., 2007. Di(2-ethylhexyl)phthalate induces hepatic tumorigenesis through a peroxisome proliferator-activated receptor alpha-independent pathway. J. Occup. Health 49, 172–182.

Kobayashi, H., Azuma, R., Yasunaga, T., 2009. Expression of excess receptors and negative feedback control of signal pathways are required for rapid activation and prompt cessation of signal transduction. Cell Commun. Signal. 7, 3.

Lee, S.S., Pineau, T., Drago, J., Lee, E.J., Owens, J.W., Kroetz, D.L., Fernandez-Salguero, P.M., Westphal, H., Gonzalez, F.J., 1995. Targeted disruption of the alpha isoform of the peroxisome proliferator-activated receptor gene in mice results in abolishment of the pleiotropic effects of peroxisome proliferators. Mol. Cell. Biol. 15, 3012–3022.

Li, L., Zhang, T., Qin, X.S., Ge, W., Ma, H.G., Sun, L.L., Hou, Z.M., Chen, H., Chen, P., Qin, G.Q., Shen, W., Zhang, X.F., 2014. Exposure to diethylhexyl phthalate (DEHP) results in a heritable modification of imprint genes DNA methylation in mouse oocytes. Mol. Biol. Rep. 41, 1227–1235.

Lovekamp-Swan, T., Davis, B.J., 2003. Mechanisms of phthalate ester toxicity in the female reproductive system. Environ. Health Perspect. 111, 139–145.

Miller, W.L., Auchus, R.J., 2011. The molecular biology, biochemistry, and physiology of human steroidogenesis and its disorders. Endocr. Rev. 32, 81–151.

Qin, X.Y., Zaha, H., Nagano, R., Yoshinaga, J., Yonemoto, J., Sone, H., 2011. Xenoestrogens down-regulate aryl-hydrocarbon receptor nuclear translocator 2 mRNA expression in human breast cancer cells via an estrogen receptor alpha-dependent mechanism. Toxicol. Lett. 206, 152–157.

Schmidt, J.S., Schaedlich, K., Fiandanese, N., Pocar, P., Fischer, B., 2012. Effects of di(2-ethylhexyl) phthalate (DEHP) on female fertility and adipogenesis in C3H/N mice. Environ. Health Perspect. 120, 1123–1129.

Suzuki, Y., Niwa, M., Yoshinaga, J., Mizumoto, Y., Serizawa, S., Shiraishi, H., 2010. Prenatal exposure to phthalate esters and PAHs and birth outcomes. Environ. Int. 36, 699–704.

Suzuki, Y., Yoshinaga, J., Mizumoto, Y., Serizawa, S., Shiraishi, H., 2012. Foetal exposure to phthalate esters and anogenital distance in male newborns. Int. J. Androl. 35, 236–244.

Swan, S.H., 2008. Environmental phthalate exposure in relation to reproductive outcomes and other health endpoints in humans. Environ. Res. 108, 177–184.

Swan, S.H., Main, K.M., Liu, F., Stewart, S.L., Kruse, R.L., Calafat, A.M., Mao, C.S., Redmon, J.B., Ternand, C.L., Sullivan, S., Teague, J.L., 2005. Decrease in anogenital distance among male infants with prenatal phthalate exposure. Environ. Health Perspect. 113, 1056–1061.

Wolf Jr., C., Lambright, C., Mann, P., Price, M., Cooper, R.L., Ostby, J., Gray Jr., L.E., 1999. Administration of potentially antiandrogenic pesticides (procymidone, linuron, iprodione, chlozolinate, p,p'-DDE, and ketoconazole) and toxic substances (dibutyl- and diethylhexyl phthalate, PCB 169, and ethane dimethane sulphonate) during sexual differentiation produces diverse profiles of reproductive malformations in the male rat. Toxicol. Ind. Health 15, 94–118.

Wu, M.T., Wu, C.F., Wu, J.R., Chen, B.H., Chen, E.K., Chao, M.C., Liu, C.K., Ho, C.K., 2012. The public health threat of phthalate-tainted foodstuffs in Taiwan: the policies the government implemented and the lessons we learned. Environ. Int. 44, 75–79.

Zacharewski, T.R., Meek, M.D., Clemons, J.H., Wu, Z.F., Fielden, M.R., Matthews, J.B., 1998. Examination of the in vitro and in vivo estrogenic activities of eight commercial phthalate esters. Toxicol. Sci. 46, 282–293.

Cytotechnology (2015) 67:191–197
DOI 10.1007/s10616-013-9686-8

TECHNICAL NOTE

Low-molecular-weight inhibitors of cell differentiation enable efficient growth of mouse iPS cells under feeder-free conditions

Kenichiro Donai · Akane Inagaki · Kyoung-Ha So · Kengo Kuroda · Hideko Sone · Masayuki Kobayashi · Katsuhiko Nishimori · Tomokazu Fukuda

Received: 23 July 2013 / Accepted: 25 December 2013 / Published online: 30 March 2014

Abstract Embryonic stem cells and induced pluripotent stem (iPS) cells are usually maintained on feeder cells derived from mouse embryonic fibroblasts (MEFs). In recent years, the cell culture of iPS cells under serum- and feeder-free conditions is gaining attention in overcoming the biosafety issues for clinical applications. In this study, we report on the use of multiple small-molecular inhibitors (i.e., CHIR99021, PD0325901, and Thiazovivin) to efficiently cultivate mouse iPS cells without feeder cells in a chemically-defined and serum-free condition. In this condition, we showed that mouse iPS cells are expressing the Nanog, Oct3/4, and SSEA-1 pluripotent markers, indicating that the culture condition is optimized to maintain the pluripotent status of iPS cells. Without these small-molecular inhibitors, mouse iPS cells required the adaptation period to start the stable cell proliferation. The application of these inhibitors enabled us the shortcut culture method for the cellular adaptation. This study will be useful to efficiently establish mouse iPS cell lines without MEF-derived feeder cells.

Keywords Induced pluripotent stem cells · Cell culture condition · Serum-free · Feeder-free · Low-molecular-weight compounds

Abbreviations

ES	Embryonic stem
iPS	Induced pluripotent stem
MEFs	Mouse embryonic fibroblasts
SSEA	Stage specific embryonic antigen
HPV	Human papilloma virus
STEMCCA	Stem cell cassette
DMEM	Dulbecco's modified Eagle's medium
KSR	Knockout serum replacement
LIF	Leukemia inhibitory factor
2i	2 Inhibitors (CHIR99021 and PD0325901)
Tzv	Thiazovivin
GSK-3β	Glycogen synthase kinase 3β
MAPK	Mitogen-activated protein kinase
ROCK	Rho-associated Kinase
PD	Population doubling

K. Donai · A. Inagaki · K.-H. So · K. Kuroda · K. Nishimori · T. Fukuda (✉)
Graduate School of Agricultural Science, Tohoku University, 1-1 Tsutsumidori-amamiyamachi, Aoba-ku, Sendai 981-8555, Japan
e-mail: tomofukuda@bios.tohoku.ac.jp

H. Sone
Environmental Exposure Research Section, Center for Environmental Risk Research, National Institute for Environmental Studies, 16-2 Onogawa, Tsukuba, Ibaraki 305-8506, Japan

M. Kobayashi
Graduate School of Bioresource Sciences, Akita Prefectural University, 241-438 Kaidobata-Nishi, Nakano, Shimoshinjo, Akita 010-0195, Japan

EBs	Embryoid bodies
AP	Alkaline phosphatase
DAPI	4′,6-Diamidino-2-phenylindole
RT	Reverse transcription
PCR	Polymerase chain reaction
cDNA	Complementary DNA

Introduction

The reprogramming of somatic cells to generate induced pluripotent stem (iPS) cells was achieved by expressing four defined transcription factors: Oct3/4, Sox2, Klf4, and c-Myc (Takahashi and Yamanaka 2006). Such iPS cells have major potential in the study and therapy of human diseases because they are capable of self-renewal and can generate all the three primary germ layers: ectoderm, mesoderm, and endoderm. iPS cells are usually maintained on feeder cells that are derived from mouse embryonic fibroblasts (MEFs) (Takahashi and Yamanaka 2006; Takahashi et al. 2007; Yu et al. 2007). However, several feeder-free conditions were developed recently especially for human embryonic stem (ES) cells and iPS cells to ensure biosafe human clinical applications (Xu et al. 2001; Amit et al. 2004; Rosler et al. 2004; Lu et al. 2006; Navarro-Alvarez et al. 2008; Miyazaki et al. 2008; Sun et al. 2009; Kitajima and Niwa 2010; Rodin et al. 2010; Hayashi et al. 2010; Fukusumi et al. 2013). Animal-derived components are relatively high risk for potential infections in clinical regenerative medicine. In addition to regenerative medicine, iPS cells are also expected to play an important role in drug screening. However, the mixed culture condition of iPS cells and the need of feeder cells make the evaluation of the effects of drugs difficult. Furthermore, the establishment of serum- and feeder-free culture conditions is significant to overcome the ethical issues related to animal experiments.

Furue et al. (2005) previously developed a serum-free, chemically defined medium called "ESF7" (now available as ESF-C), which maintains mouse ES cells on collagen-coated dishes. In this manuscript, we show that mouse iPS cells can be cultured in feeder-free conditions as well as on feeder cells using the ESF-C medium containing different kinds of low-molecular-weight cell differentiation inhibitors.

Materials and methods

Mouse iPS cell induction

A human papilloma virus-derived E6 gene was introduced to MEFs (E6-MEFs) to extend the cell proliferation until cellular senescence (Yamamoto et al. 2003). Then, STEMCCA-loxP lentiviral vector (STEMCCA means a "stem cell cassette"), which is composed of Yamanaka 4 factors and self-cleaving 2A peptides, was introduced into E6-MEFs to generate iPS cells (Sommer et al. 2009).

Cell culture

MEFs and feeder cells were cultured in MEF medium consisting of Dulbecco's modified Eagle's medium (DMEM; #08459-35, Nacalai Tesque, Kyoto, Japan) supplemented with 10 % fetal bovine serum (FBS; #12483-020, Invitrogen, Carlsbad, CA, USA) and 100× antibiotic–antimycotic mixed solution (#02892-54, Nacalai Tesque). The experimental conditions for the established mouse iPS cells are as follows: (1) mouse iPS cells were cultured on MEF feeder cells in mouse iPS cell medium [DMEM with 15 % Knockout Serum Replacement (referred to as KSR, #10828-028, Invitrogen), 0.22 mM 2-mercaptoethanol (#21438-82, Nacalai Tesque), 100 × MEM Non-essential Amino Acids Solution (#139-15651, Wako Pure Chemical Industries, Osaka, Japan), 100× antibiotic–antimycotic mixed solution and 1,000× leukemia inhibitory factor (LIF, Human, recombinant, Culture Supernatant, #125-05603, Wako Pure Chemical Industries)]; (2) mouse iPS cells were cultured on collagen (Cellmatrix Type I-A, Nitta Gelatin, Osaka, Japan)-coated dishes in ESF-C medium (#2004-05, Cell Science and Technology Institute, Sendai, Japan) containing 1,000 × LIF; (3) the same cell culture of point (2) containing three low-molecular-weight inhibitors [1.5 μM CHIR99021 (#163-24001, Wako Pure Chemical Industries), 0.5 μM PD0325901 (hereinafter the combination of these two inhibitors are referred to as 2i for short, #13034, Cayman Chemical, Ann Arbor, MI, USA), and 0.5 μM Thiazovivin (referred to as Tzv, #04-0017, Stemgent, Cambridge, MA, USA)]. The preparation of MEFs and feeder cells were described in our previous report (Donai et al. 2013).

Population doubling (PD) assay

Mouse iPS cells were seeded at a density of 5.0×10^4 cells per well in a 6-well plate. We evaluated three independent mouse iPS clones. The passages of the mouse iPS cells were carried out until one well of the 6-well plate became confluent. The cell number was counted using an automatic cell counter (Countess, Invitrogen), and the cell growth was evaluated with triplicated experiments. The passage process was repeated up to the 6th passage. Cell PD was obtained from the number of cells using the formula described in a previous report as follows: $PD = \log_2(a/b)$, where 'a' is the number of the cells counted in passage and 'b' represents the number of seeded cells (Qin et al. 2012). The results of PD assay are shown as means with standard deviations. Statistical significance was evaluated using Student's t test ($P < 0.05$).

Embryoid bodies (EBs) formation

To form EBs, $2–3 \times 10^6$ iPS cells were seeded into a Petri dish (for bacterial culture). After 3–4 days, floating EBs were picked up and transferred to 0.1 % gelatin-coated 24-well plates and cultured for 3–4 additional days. EB medium contained DMEM with 15 % FBS, 100× antibiotic–antimycotic mixed solution, 0.22 mM 2-mercaptoethanol and 100× MEM non-essential amino acids solution.

Alkaline phosphatase (AP) staining and Immunocytochemistry

Detailed method for detection of AP activity and pluripotent markers with immunocytochemistry was previously described in our publication (Donai et al. 2013). EBs on gelatin-coated dishes were stained with βIII tubulin monoclonal antibody (1:600 dilution, #MAB1637, Millipore, Billerica, MA, USA), 4′,6-diamidino-2-phenylindole (DAPI) solution (1:1,000 dilution, #340-07971, Wako Pure Chemical Industries) and Alexa Fluor 568 (1:500 dilution, #A21124, Invitrogen).

Reverse transcription (RT) and quantitative real-time polymerase chain reaction (PCR)

Total RNA was extracted from cells confluent in a 6-well plate and a Petri dish using the TaKaRa FastPure RNA Kit (#9190, TaKaRa Bio, Shiga, Japan) according to the manufacturer's protocol. Complementary DNA (cDNA) synthesis and PCR were performed in a similar way as in our previous report (Donai et al. 2013).

Results and discussion

We initially investigated whether mouse iPS cells could maintain their specific morphologies in each culture condition. Figure 1 shows the cell morphology and alkaline phosphatase (AP) staining under the conditions 1 and 2. In condition 1, using feeder cells as control, the cells showed mouse ES cell-like morphology, characterized by larger nuclei, scant cytoplasm, dome-shaped colonies, and strong positive AP staining (Fig. 1a, b). In condition 2 (collagen coating + ESF-C), mouse iPS cells showed colonies with scattering morphologies (Fig. 1c), and relatively weak AP activity (Fig. 1d). Then, we compared the cell proliferation between condition 1 and 2 using the corresponding PD values. The cell numbers in condition 1 exponentially increased (Fig. 1e, white circle) and showed aggressive growth potential represented by >1.5 population doubling per day (Fig. 1f, open bar). In condition 2, the cell growth of mouse iPS cells was remarkably delayed (Fig. 1e, black circle). The delayed iPS cell growth restored after passage three, suggesting that the cellular adaptation of mouse iPS cells to the feeder-free condition was necessary to ensure a stable cell growth. The delayed cell growth in the early passages of mouse iPS cells was apparent when the PD value was normalized by the culture day (PD per day, Fig. 1f). Furthermore, although we tried to maintain the three independent mouse iPS clones under feeder-free conditions, one of the mouse iPS clones did not show cell growth and was unable to survive in ESF-C medium (data not shown).

In condition 3, we added three inhibitors (CHIR99021, PD0325901 and Thiazovivin) to the ESF-C medium. CHIR99021 is reported as the inhibitor of glycogen synthase kinase 3β (GSK-3β) signaling, which has a large impact to maintain pluripotency of ES and iPS cells effectively (Sato et al. 2004; Besser 2004; Polychronopoulos et al. 2004; Ying et al. 2008). PD0325901 targets mitogen-activated protein kinase (MAPK/ERK kinase) (Sebolt-Leopold and Herrera 2004; Bain et al. 2007). In combination with

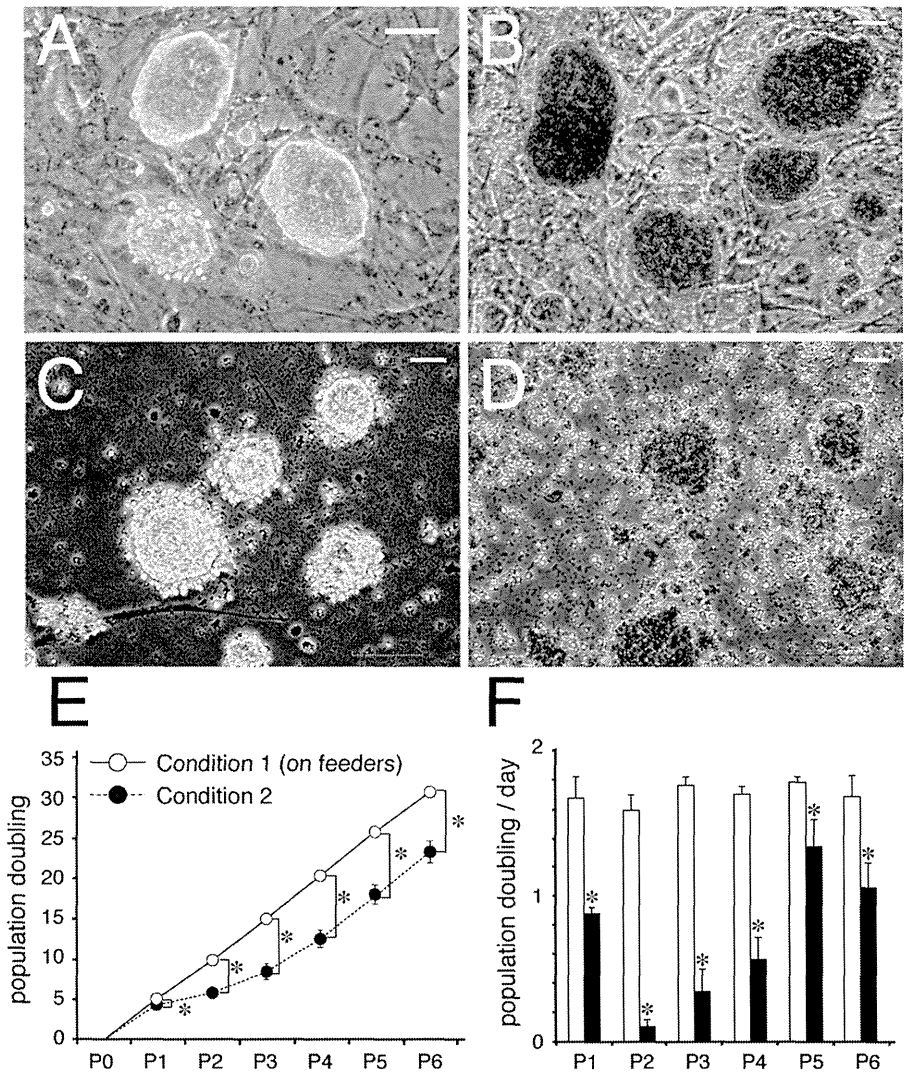

Fig. 1 Morphology of mouse iPS cell colonies in condition 1 and condition 2. *Condition 1*, on feeders in mouse iPS cell medium with LIF; *Condition 2*, on collagen-coated dishes (feeder-independent) in ESF-C medium (serum-free) with LIF. *White bar* = 50 μm. **a**, **b** Morphology of mouse iPS cell colonies (**a**) and AP staining (**b**), respectively, in condition 1, showing compact colonies and strong reactivity. **c**, **d** Morphology of mouse iPS cell colonies (**c**) and AP staining (**d**), respectively, in condition 2. Shape scattering of colonies and weak AP signals are evident. **e** The population doublings under condition 1 and condition 2. n = 3 × 3 **f** Population doubling per day. *Open* and *closed bars* correspond to condition 1 and 2, respectively. The cell growth was partly recovered at late passages in condition 2

CHIR99021, PD0325901 affects the self-renewality of ES and iPS cells to prevent cell differentiation (Lin et al. 2009). Thiazovivin acts as a Rho-associated Kinase inhibitor, which can improve the survival of ES and iPS cells from single cell dissociation (Lin et al. 2009; Xu et al. 2010). The iPS cell colonies were more rounded with clearer boundaries than those obtained under condition 2 (Fig. 2a). In agreement with the improved morphology, the reactivity against AP of the cells in the ESF-C in the presence of these three inhibitors as well as on the feeder cells became strong (Fig. 2b). Furthermore, mouse iPS cells showed enhanced cell proliferation compared to those in condition 2 (Fig. 2c). Although the cell proliferation speed in condition 3 was significantly lower than that in condition 1, the PD value of condition 3 was similar to that of condition 1. As shown in Fig. 2d, the effect of these low-molecular inhibitors (2i + Tzv) became more apparent with increasing PD per day. Based on these results, we concluded that 2i + Tzv enabled us to efficiently maintain mouse iPS cells in the chemically defined medium and in feeder-free conditions without requiring the cellular adaptation period. We evaluated the expression of pluripotent markers of mouse iPS cells under condition 3 by immunocytochemistry (Fig. 2e). The detection of the expression of markers in mouse iPS cells was in good agreement with that of mouse ES cells. Briefly, the mouse iPS cell colonies in condition 3 showed immunoreactivity against Nanog, Oct3/4, and SSEA-1 antibodies. From

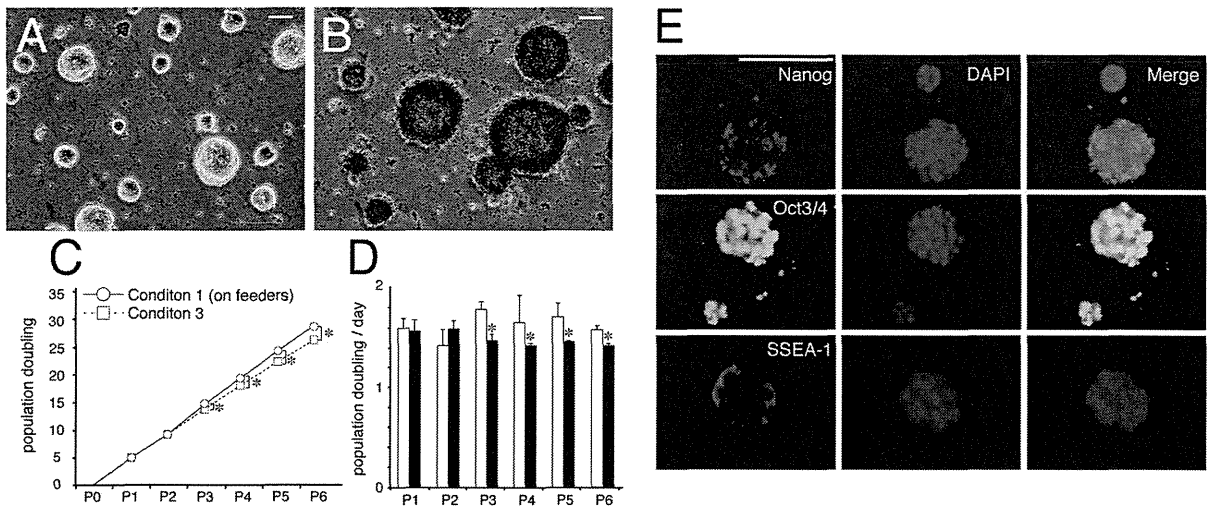

Fig. 2 The small-molecule inhibitors improve the morphology of mouse iPS cell colonies, their proliferation, and the expression of pluripotent markers. Condition 3, on collagen-coated dishes (feeder-independent) in ESF-C medium (serum-free) with LIF, 2i and Tzv. *White bar* = 50 μm. **a**, **b** Morphology of mouse iPS cell colonies and AP staining, respectively, under condition 3. The cells formed dome-shaped colonies with clear edges and displayed strong AP activity. **c** The number of population doubling under condition 1 and condition 3. The growth speed in condition 3 showed enhanced proliferation similar to that of condition 1. **d** Population doubling per day. Mouse iPS cells showed good cell proliferation starting from early passages. *Open* and *closed bars* represent condition 1 and 3, respectively. **e** Expression of pluripotent markers in mouse iPS cells. Nanog- and Oct 3/4-positive staining, which could be overlapped with DAPI *blue* counterstaining, was detected in the nuclei. Stage-specific embryonic antigen (SSEA)-1 protein localizes at the cell surface. *White bar* = 100 μm. (Color figure online)

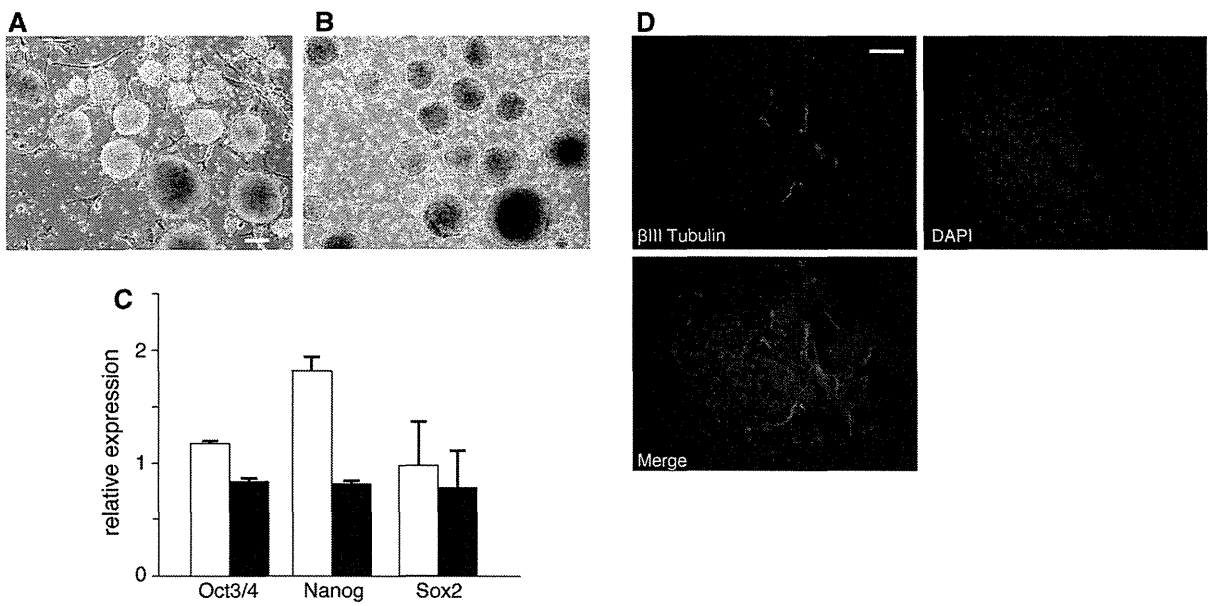

Fig. 3 In vitro differentiation of iPS cells. **a**, **b** Morphology of EBs floating in a Petri dish after 4 days incubation. *Left panel* (**a**) EBs derived from iPS cells cultivated under condition 1; *Right panel* (**b**) EBs derived from iPS cells cultivated under condition 3. *White bar* 100 μm. **c** Detection of stem cell-specific genes by real-time quantitative polymerase chain reaction (RT-qPCR) between iPS cells and EBs in condition 3. *White column* iPS cells (undifferentiated state); *Black column* EBs (differentiated state). n = 3 **d** immunostaining of βIII tubulin (ectoderm) marker in EBs cultivated 4 days on gelatin-coated dishes derived from condition 3. *White bar* 50 μm

these data, we concluded that our mouse iPS cells maintained a pluripotent state even in the absence of serum and feeder cells.

To validate whether iPS cells have differentiation capacity in feeder-independent culture, we tried to form EBs after incubation in condition 1 and 3. We could not detect any difference in EBs formation between condition 1 and 3 (Fig. 3a, b). After EBs formation, we detected lower expression levels of stem cell-specific genes compared with pluripotent state (Fig. 3c). Furthermore, we also detected βIII tubulin (ectoderm) marker by immunostaining (Fig. 3d). These findings indicate that differentiation capacity is still intact even in chemically-defined and serum-free condition.

In this study, we demonstrated the efficient expansion of mouse iPS cells on collagen-coated dishes under serum- and feeder-free conditions in combination with three small-molecule cell differentiation inhibitors. We could not observe any morphological or cell proliferation change until passage 10. We also confirmed the effect of the inhibitors on the cell growth of mouse ES cell line E14tg2a. They expectedly showed growth pattern similar to that of iPS cells under the presence of these inhibitors (data not shown). Collagen coating is a simple method and does not require special techniques. This method provides a useful means for using mouse iPS cells to assess novel drugs and animal-derived components without adaptation periods.

Acknowledgments We thank Dr. Gustavo Mostoslavsky (Boston University School of Medicine) for providing the STEMCCA-loxP lentiviral vector. We also thank the technical supports and suggestion from and Dr. Takehiro Ito and Ms. Yukiko Kitamura (Cell Science and Technology Institute). This work was supported by research grants from the Tojuro Iijima Foundation for Food Science and Technology, Asahi Group Foundation and a JSPS grant (KAKENHI, #23650587 and #25640117).

References

Amit M, Shariki C, Margulets V, Itskovitz-Eldor J (2004) Feeder layer- and serum-free culture of human embryonic stem cells. Biol Reprod 70:837–845. doi:10.1095/biolreprod.103.021147

Bain J, Plater L, Elliott M, Shpiro N, Hastie CJ, McLauchlan H, Klevernic I, Arthur JS, Alessi DR, Cohen P (2007) The selectivity of protein kinase inhibitors: a further update. Biochem J 408:297–315. doi:10.1042/BJ20070797

Besser D (2004) Expression of nodal, lefty-a, and lefty-B in undifferentiated human embryonic stem cells requires activation of Smad2/3. J Biol Chem 279:45076–45084. doi:10.1074/jbc.M404979200

Donai K, Kuroda K, Guo Y, So KH, Sone H, Kobayashi M, Nishimori K, Fukuda T (2013) Establishment of a reporter system to monitor silencing status in induced pluripotent stem cell lines. Anal Biochem 443:104–112. doi:10.1016/j.ab.2013.08.014

Fukusumi H, Shofuda T, Kanematsu D, Yamamoto A, Suemizu H, Nakamura M, Yamasaki M, Ohgushi M, Sasai Y, Kanemura Y (2013) Feeder-free generation and long-term culture of human induced pluripotent stem cells using pericellular matrix of decidua derived mesenchymal cells. PLoS ONE 8:e55226. doi:10.1371/journal.pone.0055226

Furue M, Okamoto T, Hayashi Y, Okochi H, Fujimoto M, Myoishi Y, Abe T, Ohnuma K, Sato GH, Asashima M, Sato JD (2005) Leukemia inhibitory factor as an anti-apoptotic mitogen for pluripotent mouse embryonic stem cells in a serum-free medium without feeder cells. In Vitro Cell Dev Biol Anim 41:19–28. doi:10.1290/0502010.1

Hayashi Y, Chan T, Warashina M, Fukuda M, Ariizumi T, Okabayashi K, Takayama N, Otsu M, Eto K, Furue MK, Michiue T, Ohnuma K, Nakauchi H, Asashima M (2010) Reduction of N-glycolylneuraminic acid in human induced pluripotent stem cells generated or cultured under feeder- and serum-free defined conditions. PLoS ONE 5:e14099. doi:10.1371/journal.pone.0014099

Kitajima H, Niwa H (2010) Clonal expansion of human pluripotent stem cells on gelatin-coated surface. Biochem Biophys Res Commun 396:933–938. doi:10.1016/j.bbrc.2010.05.026

Lin T, Ambasudhan R, Yuan X, Li W, Hilcove S, Abujarour R, Lin X, Hahm HS, Hao E, Hayek A, Ding S (2009) A chemical platform for improved induction of human iPSCs. Nat Methods 6:805–808. doi:10.1038/nmeth.1393

Lu J, Hou R, Booth CJ, Yang SH, Snyder M (2006) Defined culture conditions of human embryonic stem cells. Proc Natl Acad Sci USA 103:5688–5693. doi:10.1073/pnas.0601383103

Miyazaki T, Futaki S, Hasegawa K, Kawasaki M, Sanzen N, Hayashi M, Kawase E, Sekiguchi K, Nakatsuji N, Suemori H (2008) Recombinant human laminin isoforms can support the undifferentiated growth of human embryonic stem cells. Biochem Biophys Res Commun 375:27–32. doi:10.1016/j.bbrc.2008.07.111

Navarro-Alvarez N, Soto-Gutierrez A, Yuasa T, Yamatsuji T, Shirakawa Y, Nagasaka T, Sun SD, Javed MS, Tanaka N, Kobayashi N (2008) Long-term culture of Japanese human embryonic stem cells in feeder-free conditions. Cell Transpl 17:27–33

Polychronopoulos P, Magiatis P, Skaltsounis AL, Myrianthopoulos V, Mikros E, Tarricone A, Musacchio A, Roe SM, Pearl L, Leost M, Greengard P, Meijer L (2004) Structural basis for the synthesis of indirubins as potent and selective inhibitors of glycogen synthase kinase-3 and cyclin-dependent kinases. J Med Chem 47:935–946. doi:10.1021/jm031016d

Qin XY, Fukuda T, Yang L, Zaha H, Akanuma H, Zeng Q, Yoshinaga J, Sone H (2012) Effects of bisphenol a exposure on the proliferation and senescence of normal human

mammary epithelial cells. Cancer Biol Ther 13:296–306. doi:10.4161/cbt.18942

Rodin S, Domogatskaya A, Strom S, Hansson EM, Chien KR, Inzunza J, Hovatta O, Tryggvason K (2010) Long-term self-renewal of human pluripotent stem cells on human recombinant laminin-511. Nat Biotechnol 28:611–615. doi:10.1038/nbt.1620

Rosler ES, Fisk GJ, Ares X, Irving J, Miura T, Rao MS, Carpenter MK (2004) Long-term culture of human embryonic stem cells in feeder-free conditions. Dev Dyn 229:259–274. doi:10.1002/dvdy.10430

Sato N, Meijer L, Skaltsounis L, Greengard P, Brivanlou AH (2004) Maintenance of pluripotency in human and mouse embryonic stem cells through activation of Wnt signaling by a pharmacological GSK-3-specific inhibitor. Nat Med 10:55–63. doi:10.1038/nm979

Sebolt-Leopold JS, Herrera R (2004) Targeting the mitogen-activated protein kinase cascade to treat cancer. Nat Rev Cancer 4:937–947. doi:10.1038/nrc1503

Sommer CA, Stadtfeld M, Murphy GJ, Hochedlinger K, Kotton DN, Mostoslavsky G (2009) Induced pluripotent stem cell generation using a single lentiviral stem cell cassette. Stem Cells 27:543–549. doi:10.1634/stemcells.2008-1075

Sun N, Panetta NJ, Gupta DM, Wilson KD, Lee A, Jia F, Hu S, Cherry AM, Robbins RC, Longaker MT, Wu JC (2009) Feeder-free derivation of induced pluripotent stem cells from adult human adipose stem cells. Proc Natl Acad Sci USA 106:15720–15725. doi:10.1073/pnas.0908450106

Takahashi K, Yamanaka S (2006) Induction of pluripotent stem cells from mouse embryonic and adult fibroblast cultures by defined factors. Cell 126:663–676. doi:10.1016/j.cell.2006.07.024

Takahashi K, Tanabe K, Ohnuki M, Narita M, Ichisaka T, Tomoda K, Yamanaka S (2007) Induction of pluripotent stem cells from adult human fibroblasts by defined factors. Cell 131:861–872. doi:10.1016/J.Cell.11.019

Xu C, Inokuma MS, Denham J, Golds K, Kundu P, Gold JD, Carpenter MK (2001) Feeder-free growth of undifferentiated human embryonic stem cells. Nat Biotechnol 19:971–974. doi:10.1038/nbt1001-971

Xu Y, Zhu X, Hahm HS, Wei W, Hao E, Hayek A, Ding S (2010) Revealing a core signaling regulatory mechanism for pluripotent stem cell survival and self-renewal by small molecules. Proc Natl Acad Sci USA 107:8129–8134. doi:10.1073/pnas.1002024107

Yamamoto A, Kumakura S, Uchida M, Barrett JC, Tsutsui T (2003) Immortalization of normal human embryonic fibroblasts by introduction of either the human papillomavirus type 16 E6 or E7 gene alone. Int J Cancer 106:301–309. doi:10.1002/ijc.11219

Ying QL, Wray J, Nichols J, Batlle-Morera L, Doble B, Woodgett J, Cohen P, Smith A (2008) The ground state of embryonic stem cell self-renewal. Nature 453:519–523. doi:10.1038/nature06968

Yu J, Vodyanik MA, Smuga-Otto K, Antosiewicz-Bourget J, Frane JL, Tian S, Nie J, Jonsdottir GA, Ruotti V, Stewart R, Slukvin II, Thomson JA (2007) Induced pluripotent stem cell lines derived from human somatic cells. Science 318:1917–1920. doi:10.1126/science.1151526

Toxicology Letters 228 (2014) 207–215

Contents lists available at ScienceDirect

Toxicology Letters

journal homepage: www.elsevier.com/locate/toxlet

Effects of PAMAM dendrimers in the mouse brain after a single intranasal instillation

Tin-Tin Win-Shwe[a], Hideko Sone[b,*], Yoshika Kurokawa[b], Yang Zeng[b], Qin Zeng[b], Hiroshi Nitta[a], Seishiro Hirano[b]

[a] Center for Environmental Health Sciences, National Institute for Environmental Studies, 16-2 Onogawa, Tsukuba, Ibaraki 305-8506, Japan
[b] Center for Environmental Risk Research, National Institute for Environmental Studies, 16-2 Onogawa, Tsukuba, Ibaraki 305-8506, Japan

HIGHLIGHTS

- A single dose of PAMAM dendrimers was intranasally administered to 8-week old male BALB/c mice.
- Gene expression profiling was examined in the olfactory bulb, hippocampus, and cerebral cortex of the mouse brain.
- Brain derived-neurotrophic factor mRNA was up-regulated in the hippocampus and cerebral cortex in PAMAM-treated mice.
- PAMAM dendrimers may reach the brain after intranasal instillation and induce neuronal effects.

ARTICLE INFO

Article history:
Received 28 October 2013
Received in revised form 20 April 2014
Accepted 22 April 2014
Available online 9 May 2014

Keywords:
Nanomaterials
PAMAM dendrimers
Biomarkers
Neurotoxicity
Mouse

ABSTRACT

Dendrimers are highly branched spherical nanomaterials produced for use in diagnostic and therapeutic applications such as a drug delivery system. The toxicological profiles of dendrimers are largely unknown. We investigated the *in vivo* effects of nasal exposure to polyamidoamine (PAMAM) dendrimers on their effects on neurological biomarkers in the mouse brain. A single dose of PAMAM dendrimers (3 or 15 μg/mouse) was intranasally administered to 8-week old male BALB/c mice. Twenty-four hours after administration, the olfactory bulb, hippocampus, and cerebral cortex were collected and potential biomarkers in the blood and brain were examined using blood marker, microarray and real-time RT-PCR analyses. No remarkable changes in standard serum biochemical markers were observed in the blood. A microarray analysis showed the alterations of the genes expression level related to pluripotent network, serotonin-anxiety pathway, TGF-beta receptor signaling, prostaglandin synthesis-regulation, complement-coagulation cascades, and chemokine-signaling pathway and non-odorant GPCR signaling pathways in brain tissues. Brain derived-neurotrophic factor mRNA was up-regulated in the hippocampus and cerebral cortex in mice treated with a high dose of dendrimers. These findings suggest that PAMAM dendrimers may reach the brain *via* the systemic circulation or an olfactory nerve route after intranasal instillation, and indicate that a single intranasal administration of PAMAM dendrimers may potentially lead to neuronal effects by modulating the gene expression of brain-derived neurotrophic factor signaling pathway.

1. Introduction

Dendrimers are generally described as macromolecules with highly branched structures that provide a high degree of surface functionalities and interior cavities. Dendrimers are very promising nanomaterials for therapeutic and diagnostic purposes (Lee et al., 2005; Tekade et al., 2009). Because of their multivalent and monodisperse characters, dendrimers have been a topic of interest in the fields of chemistry and biology, especially for applications in drug delivery, gene therapy, and chemotherapy (Buhleier et al., 1978; Newkome et al., 1985; Tomalia et al., 1985). Current understanding of the toxicological and pharmacological effects of dendrimers is limited, and an improved understanding of the toxicities of various dendrimer formulations is essential. Toxicological and pharmacokinetic investigations examining the cytotoxicity of dendrimers and the immune response to dendrimers are needed

* Corresponding author. Center for Environmental Risk Research National Institute for Environmental Studies 16-2, Onogawa, Tsukuba, Ibaraki 305-8506, Japan Tel.: +81 29 850 2464; fax: +81 29 850 2546.
E-mail address: hsone@nies.go.jp (H. Sone).

http://dx.doi.org/10.1016/j.toxlet.2014.04.020
0378-4274/

to design dendrimers for therapeutic and diagnostic uses. Although attention has been paid to clinical applications, little is known about their biological safety. Therefore, the possible adverse effects on humans and the environment needed to be evaluated.

Nanoparticles are divided into combustion-derived nanoparticles and manufactured or engineered nanoparticles. Previously, our laboratory has demonstrated the effects of the intranasal instillation of carbon black nanoparticles on inflammatory mediators in the mouse brain (Win-Shwe et al., 2006) and the effects of inhalation exposure to nanoparticle-rich diesel exhaust on the expression level of memory function-related genes and hippocampal dependent spatial and non-spatial learning behavior (Win-Shwe et al., 2008a, 2009, 2012a, 2012b; Win-Shwe et al., 2011). Nanotechnology has been advanced increasingly and among the well-developed nanomaterials, polyamidoamine (PAMAM) dendrimers are widely used for various biomedical applications including drug delivery, molecular imaging, and gene therapy (Na et al., 2006; Zhou et al., 2006; Dear et al., 2006; Swanson et al., 2008). PAMAM dendrimers are synthesized using a divergent method starting from ammonia or ethylenediamine initiator core reagents (Pushkar et al., 2006). Currently, many *in vitro* studies using mammalian cell lines have shown the cytotoxicity of PAMAM dendrimers (Lee et al., 2009; Naha et al., 2010; Mukherjee et al., 2010a, 2010b). It was reported that PAMAM dendrimers can make a hole in the plasma membrane, which may trigger membrane disruption (Hong et al., 2004; Leroueil et al., 2008). Toxicity has also been shown to increase with increasing dendrimer generation (Naha et al., 2009). However, reports describing the *in vivo* toxicological assessment of dendrimers are limited. These findings prompted us to investigate the toxicological effects of dendrimers.

Regarding recent *in vivo* studies of nanomaterials, the intranasal instillation of titanium dioxide nanoparticles for 90 consecutive days was reported to induce oxidative stress and to trigger the overproliferation of spongiocytes and to induce hemorrhage in the mouse brain (Ze et al., 2013). Moreover, a kinetic study has reported that zinc oxide nanoparticles have a higher absorption and a more extensive organ distribution, compared with titanium dioxide nanoparticles, after 13 weeks of oral exposure (Cho et al., 2013).

We hypothesized that since dendrimers are nano-sized particles, they could potentially reach the brain *via* an olfactory nerve or through the systemic circulation following intranasal instillation, as previously described in our other studies (Win-Shwe et al., 2006, 2008b); once they have reached the brain, they might affect the immune system or induce an inflammatory response. Therefore, we selected the olfactory bulb to detect the effects of intranasally instilled dendrimers. Other areas, such as the hippocampus and the cerebral cortex, were selected to enable a comparison with our previous findings for neuro-immune biomarkers in those areas after the intranasal instillation of nanoparticle carbon black. Therefore, in the present study, to determine whether PAMAM dendrimers cause toxicity in an animal model, we used male BALB/c mice to assess the neurotoxic effects of the single intranasal administration of PAMAM dendrimers on neurological biomarkers in the mouse brain. We also assessed the genes affected by PAMAM dendrimers using microarray analyses.

2. Materials and methods

2.1. Nanomaterials

PAMAM dendrimer (1,4-diaminobutane core, generation 4, 10% w/w methanol solution) was purchased from Sigma–Aldrich (product number 683507, PAMAM-amine dendrimer, NH_2 surface type, positive charge; St. Louis, MO, USA). The dendrimer particles were desiccated after the spontaneous volatilization of methanol and were re-suspended in ultrapure water (Milli-Q). Aliquots were then used in the experiments after storage for more than one day to enable a thorough distribution of the particles.

2.2. Characterization of PAMAM-NH_2 dendrimers

According to the manufacturer, the primary size of PAMAM-NH_2 dendrimers (G4) is 4.5 nm in diameter; each dendrimer has 64 (amine) surface groups and a molecular weight of 14,234 Da. A schematic diagram of the PAMAM dendrimer (G4) that was used in the present study and the distribution of the hydrodynamic diameter of PAMAM dendrimers in ultrapure water are shown in Fig. 1. In the present study, we selected G4 dendrimers because our *in vitro* pilot study had shown that among the PAMAM dendrimers, the G4 dendrimers were associated with potential cytotoxicity in human neural progenitor cells. The particle size distributions were calculated using the light intensity distribution data. For measurement, the whole range of operations from the detection of scattered light intensity distribution patterns to the calculation of the particle size distribution was performed. Using Zeta Potential and Particle Analyzer (Otsuka Electronics ELSZ-2, Osaka, Japan) we first measured the particle size distribution of PAMAM in 100% methanol (mean size, 3.4 ± 0.9 nm); after removing methanol using nitrogen purging, PAMAM was again distributed in ultrapure water (mean size, 5.7 ± 1.4 nm in first peak; 976 ± 391 nm in second peak). Then, the PAMAM was stored in ultrapure water overnight to allow the thorough dispersal of the PAMAM dendrimers (mean size, 5.6 ± 2.3 nm; second peak was disappeared) prior to use in the intranasal instillation experiments.

2.3. Animals

Male BALB/c mice (7 weeks old) were purchased from Japan Clea Co. (Tokyo, Japan). Eight-week-old mice were used in the experiments. Food and water were given *ad libitum*. The mice were allotted into three groups: a control group ($n = 5$), a low-dose dendrimer-treated group ($n = 5$) and a high-dose dendrimer-treated group ($n = 5$). The mice were housed in plastic cages under controlled environmental conditions (temperature, 22 ± 0.5 °C; humidity, 50 ± 5%; lights on 07:00–19:00 h). The experimental protocols were approved by the Ethics Committee of the Animal Care and Experimentation Council of the National Institute for Environmental Studies (NIES), Japan.

2.4. Administration of dendrimers

The intranasal route is widely used for the administration of pharmaceutical agents and vaccines. We considered a single intranasal instillation dose of 15 μg to be a "high dose" and 3 μg to be a "low dose" of dendrimers in the present study.

The mice were treated with a single dose of 30 μL PAMAM dendrimers (3 or 15 μg/mouse) into both nostrils under light sodium pentobarbital anesthesia. The control mice were given ultrapure water only.

2.5. Serum biochemical assay

Twenty-four hours after the intranasal instillation of PAMAM dendrimers, blood was drawn from the heart of each mouse under deep sodium pentobarbital anesthesia to examine various biochemical markers. The blood urea nitrogen (BUN), creatinine (CRE), total cholesterol (T-CHO), triglyceride (TG), pyruvic acid (PA), and lactic acid (LA) levels were analyzed using enzymatic methods, while the sodium (Na) and potassium (K) levels were analyzed using ion electrode methods. Then, the calcium (Ca) and iron (Fe) levels were analyzed using colorimetric assays, and the aspartate transaminase (AST), alanine transaminase (ALT), and lactate dehydrogenase (LDH) levels were analyzed using enzyme activity assays.

2.6. Microarray analyses and bioinformatics

To detect gene expression changes in the olfactory bulb, hippocampus, and cerebral cortex after a single intranasal instillation of dendrimers, microarray analyses were performed using an Agilent microarray (SurePrint G3 8×60 K mouse; Agilent Technologies, Inc., Santa Clara, CA, USA). An equivalent amount of total RNAs from six mice were pooled from each group and were used for microarray analyses. The arrays were hybridized and scanned in accordance with the manufacturer's directions at the facility of Hokkaido System Science Co., Ltd. (Sapporo, Japan). The expression values were normalized according to a median of 75%, filtered with a flag tag to remove genes which expression levels were low, and statistically analyzed using GeneSpring GX12.01 software (Agilent Technologies). Alterations in gene expression were represented as the $\log_2$ ratio. Finding pathways that integrated the collected biological knowledge were also analyzed using the GeneSpring software. Microarray data was submitted to GEO (Gene Expression Omnibus in National Center for Biotechnology Information, http://www.ncbi.nlm.nih.gov/geo/) and was registered as GSE56159.

2.7. Quantification of mRNA expression levels

Twenty-four hours after dendrimer instillation, the mice were sacrificed under deep pentobarbital anesthesia and the olfactory bulb, hippocampus, and cerebral cortex were collected from each group of mice and frozen quickly in liquid nitrogen, then stored at −80 °C until the total RNA was extracted. Briefly, total RNA extraction from the tissue samples was performed using the BioRobot EZ-1 and EZ-1 RNA tissue mini-kits (Qiagen GmbH, Hilden, Germany). Then, the purity of the total RNA

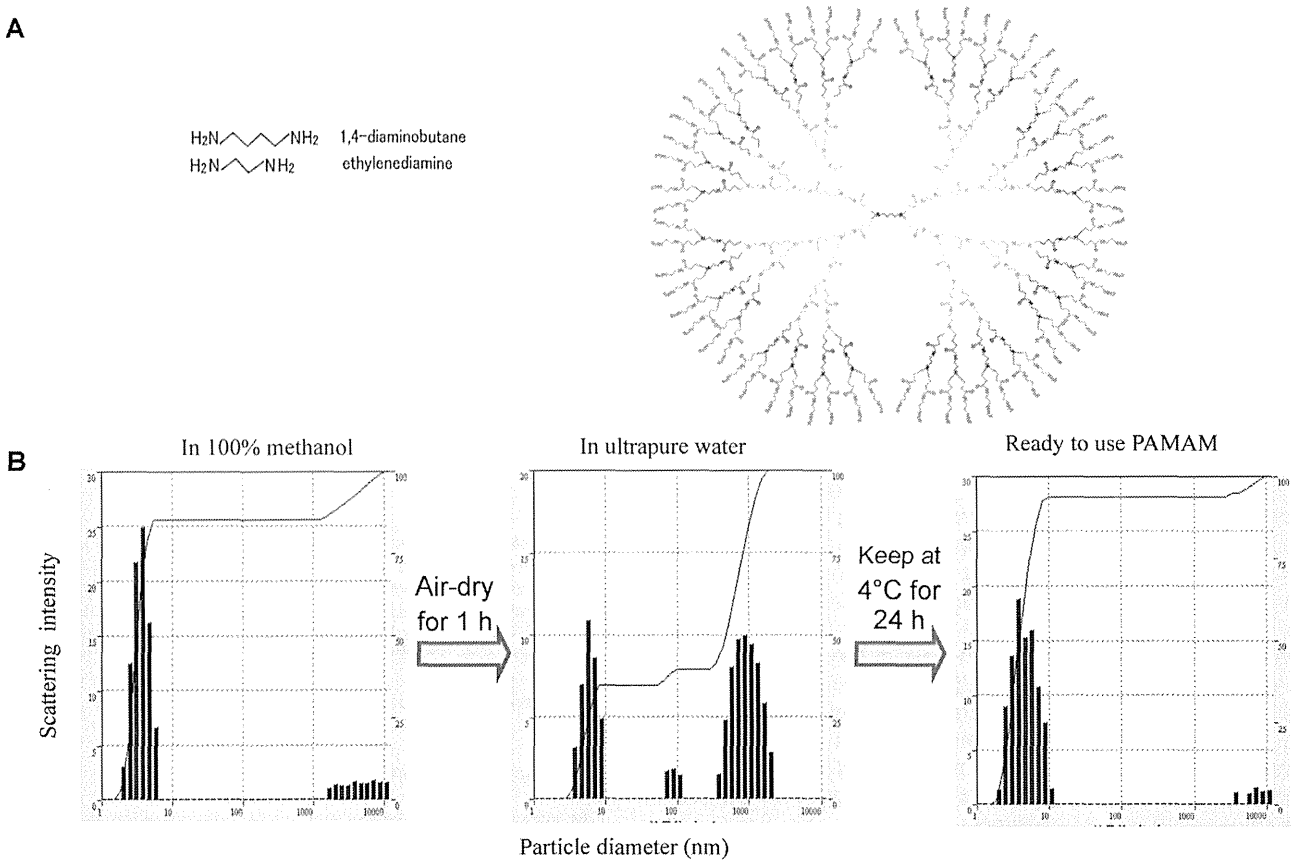

Fig. 1. (A) Schematic diagram of PAMAM dendrimer-NH_2 (G4) used in the present study and (B) distribution of hydrodynamic diameter of PAMAM dendrimer-NH_2 in ultrapure water. The particle size distributions were calculated using the light intensity distribution data. For the measurements, the whole range of operations from the detection of scattered light intensity distribution patterns to the calculation of the particle size distribution was performed. First, we measured the particle size distribution of PAMAM in 100% methanol; after the removal of methanol by air drying, the PAMAM dendrimers were again distributed in ultrapure water. Then, PAMAM was stored in ultrapure water overnight at 4 °C to allow the thorough dispersal of the PAMAM dendrimers, which were then used for the intranasal instillation experiments.

was examined, and the quantity was estimated using the ND-1000 NanoDrop RNA Assay protocol (NanoDrop, Wilmington, DE, USA), as described previously (Win-Shwe et al., 2008b). Next, we performed first-strand cDNA synthesis from the total RNA using SuperScript RNase H⁻Reverse Transcriptase II (Invitrogen, USA), according to the manufacturer's protocol. We examined the mRNA expressions using a quantitative real-time RT-PCR method and the Applied Biosystems (ABI) Prism 7000 Sequence Detection System (Applied Biosystems Inc., Foster City, CA, USA). The tissue 18S rRNA level was used as an internal control. Some primers (cyclooxygenase 2 [COX2], NM_011198; heme oxygenase [HO] 1, NM_010442; interleukin [IL-1] β, NM_008361; nuclear factor kappa B [NFκB], NM_025937; and brain-derived neurotrophic factor [BDNF], NM_007540) were purchased from Qiagen, Sample & Assay Technologies. Other primers were designed in our laboratory: 18S (forward 5′-TACCACATCCAAGAAGGCAG-3′, reverse 5′-TGCCCTCCAATGGATCCTC-3′), and nerve growth factor [NGF] (forward 5′-TGGGCTTCAGGGACAGAGTC-3′, reverse 5′-CAGCTTTCTATACTGGCCGCAG-3′). Data were analyzed using the comparative threshold cycle method. The relative mRNA expression levels were expressed as mRNA signals per unit of 18S rRNA (Rn18s) expression.

2.8. Preparation of histological brain slices

Twenty-four hours after dendrimer instillation, the brains were removed from two mice in each of the control and high-dose exposure groups after the animals had been deeply anesthetized with sodium pentobarbital; the brains were then fixed with 10% formalin. The fixed brains were dehydrated using a graded series of ethanol, cleared with xylene, and embedded in paraffin. Coronal paraffin sections were cut at a thickness of 4 μm using a microtome and were mounted on 3-aminopropyltriethoxysilane-coated glass slides and stained with hematoxylin and eosin (H&E) for histological examination.

2.9. Statistical analysis

All the data were expressed as the mean ± standard error (S.E.). The statistical analysis was performed using the StatMate II statistical analysis system for Microsoft Excel, Version 5.0 (Nankodo Inc., Tokyo, Japan). The dose-response data were analyzed using a one-way analysis of variance with a *post hoc* analysis using the Bonferroni/Dunn method. Differences were considered significant at $P < 0.05$.

3. Results

3.1. Serum biochemical markers

Standard serum biochemical markers were monitored after acute PAMAM dendrimer treatment. The BUN, CRE, Na, K, Fe, AST, ALT, LDH, T-CHO, TG, PA, and LA levels did not differ significantly between the control and the dendrimer-treated mice (Table 1). These findings indicate that no general toxicity was observed in the present study.

3.2. Microarray analyses

2506 to 5027 genes with $\log_2$ fold changes >1.5 or <−1.5 from the three brain areas were selected and analyzed by the SEA (Single Experiment Analysis) of Genespring to find matching genes out of functional pathways in Wikipathway which was downloaded into GeneSpring database. The SEA pathway analysis can find functional annotation pathway listed by those matching genes between experimental data and genes in the known pathway of Wikipathway. The pathway analysis showed pluripotent network, serotonin-anxiety pathway, TGF-beta receptor signaling, prostaglandin synthesis-regulation, complement-coagulation cascades, blood coagulation cascade and chemokine-signaling pathway and non-odorant GPCR signaling pathways among a more than 1.5-fold up-regulation or

Table 1
Standard serum biochemical markers from dendrimer-treated mice.

	BUN (mg/dL)	CRE (mg/dL)	Na (mEq/L)	K (mEq/L)	Fe (μg/dL)	AST (IU/L)	ALT (IU/L)	LDH (IU/L)	T-CHO (mg/dL)	TG (mg/dL)	PA (mg/dL)	LA (mg/dL)
Control	13.8 ± 4.2	0.05 ± 0.0	150.0 ± 24.7	3.1 ± 0.7	78.2 ± 30.3	58.2 ± 33.6	17.8 ± 6.7	187.8 ± 82.3	29.8 ± 9.8	48.6 ± 26.7	0.23 ± 0.1	20.1 ± 6.2
Low dose	14.5 ± 4.5	0.05 ± 0.0	162.8 ± 2.2	2.8 ± 1.0	68.4 ± 24.8	45.6 ± 15.8	19.0 ± 5.6	171.8 ± 54.1	29.8 ± 14.2	31.4 ± 13.0	0.12 ± 0.1	16.2 ± 12.0
High dose	19.4 ± 6.4	0.08 ± 0.1	164.0 ± 1.2	3.3 ± 0.8	68.2 ± 24.3	48.2 ± 9.6	21.4 ± 1.0	170.2 ± 22.2	38.8 ± 15.0	50.8 ± 19.5	0.12 ± 0.3	28.3 ± 24.2

Data represents the mean ± SD ($n = 5$ from each group).
Abbreviations: blood urea nitrogen; BUN; creatinine; CRE; sodium; Na; potassium; K; iron; Fe; aspartate transaminase; AST; alanine transaminase, ALT; lactate dehydrogenase, LDH; total cholesterol, T-CHO, triglyceride, TG; pyruvic acid, PA; lactic acid, LA.

Table 2
Functional annotation pathway listed by pathway analysis that found matching genes between experimental data and genes in the known pathway of Wikipathway.

Tissues	Functional annotated pathways of Wikipathway	*P*-value	Matched gene entities	Gene entities in the pathway
Olfactory bulb	Mm_PluriNetWork_WP1763_41345	0.00150	12	291
	Mm_serotonin_and_anxiety_WP2141_47355	0.00192	3	18
	Mm_TGF-beta_Receptor_Signaling_Pathway_WP258_41259	0.00192	8	150
	Mm_Alpha6-Beta4_Integrin_Signaling_Pathway_WP488_41271	0.00326	5	67
	Mm_ErbB_signaling_pathway_WP1261_41378	0.00486	4	46
	Mm_EGFR1_Signaling_Pathway_WP572_41396	0.00493	8	176
	Mm_Insulin_Signaling_WP65_41286	0.00945	7	159
Cerebral Cortex	Mm_Prostaglandin_Synthesis_and_Regulation_WP374_41394	0.00000	12	31
	Mm_Complement_and_Coagulation_Cascades_WP449_41301	0.00000	13	62
	Mm_PluriNetWork_WP1763_41345	0.00025	28	291
	Mm_metapathway_biotransformation_WP1251_41349	0.00069	16	143
	Mm_Eicosanoid_Synthesis_WP318_41263	0.00149	5	19
	Mm_Monoamine_GPCRs_WP570_48232	0.00386	6	33
	Mm_TGF-beta_Receptor_Signaling_Pathway_WP258_41259	0.00458	15	150
	Adherens junction	0.00478	3	8
	Mm_Androgen_Receptor_Signaling_Pathway_WP252_47768	0.00577	12	112
	Mm_Nuclear_Receptors_WP509_41291	0.00789	6	38
Hippocampus	Mm_Chemokine_signaling_pathway_WP2292_53116	0.00010	16	193
	Mm_TGF_Beta_Signaling_Pathway_WP113_41270	0.00013	8	52
	Mm_Non-odorant_GPCRs_WP1396_41256	0.00013	20	267
	Mm_MAPK_signaling_pathway_WP493_47770	0.00086	13	159
	Mm_Type_II_interferon_signaling_(IFNG)_WP1253_48389	0.00257	5	34
	Mm_Monoamine_GPCRs_WP570_48232	0.00257	5	33
	Mm_PluriNetWork_WP1763_41345	0.00562	17	291
	Mm_Insulin_Signaling_WP65_41286	0.00674	11	159
	Mm_Tryptophan_metabolism_WP79_47759	0.00819	5	44

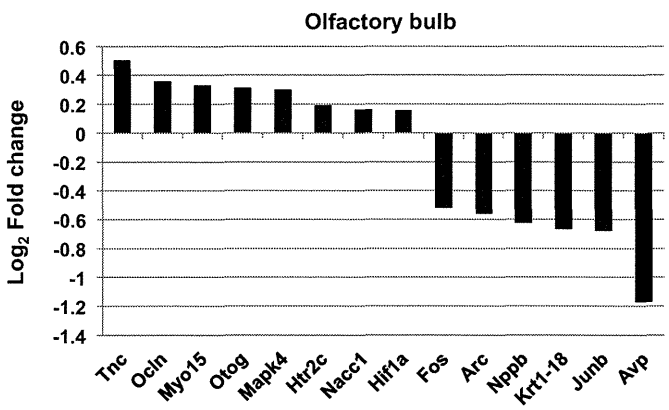

Fig. 2. Microarray analyses in the olfactory bulb. The relative mRNA expression was shown as the log fold-change referring to the control RNA level. Each bar represents a value of pooled RNAs from six mice per group.

down-regulation in the gene expression level (Table 2). Top 15–26 altered-gene expressions were shown in the olfactory bulb (Fig. 2), cerebral cortex (Fig. 3) and hippocampus (Fig. 4) of mice treated with high-dose dendrimers, compared with the levels in the control mice. Interestingly, pluripotent network and TGF-beta receptor signaling related-genes were commonly responsive among three brain areas by exposure to PAMAM dendrimers. In the hippocampus, we found that Mapk4, Bdnf and Htr2 C were up-regulated (Fig. 4A) and Bdnf-Mapk-related signaling pathway was expressed in Fig 4B.

3.3. Inflammatory markers and neurotrophins in the brain

To detect the inflammatory and immune responses after dendrimer treatment, we examined the gene expression levels of the potent inflammatory mediator *Cox2*, the oxidative stress marker *Ho1*, the immune cell cytokine *Il-1β*, and the transcription factor *NfκB* in the olfactory bulb, hippocampus, and cerebral cortex (Table 3). In addition, as we found that Bdnf expression was up-regulated in hippocampus in our microarray results, we also examined the expression levels of neurotrophins, such as *Ngf* and *Bdnf*, and found that the Bdnf mRNA levels were significantly increased in the hippocampus and cerebral cortex of the high-dose dendrimer-treated mice ($P < 0.05$, Fig. 5).

3.4. Histological findings

We examined the morphological and pathological changes in the olfactory bulb and hippocampus after a single exposure to dendrimers. We did not find any obvious significant changes in the brains of mice exposed to dendrimers, compared with the control group (data not shown).

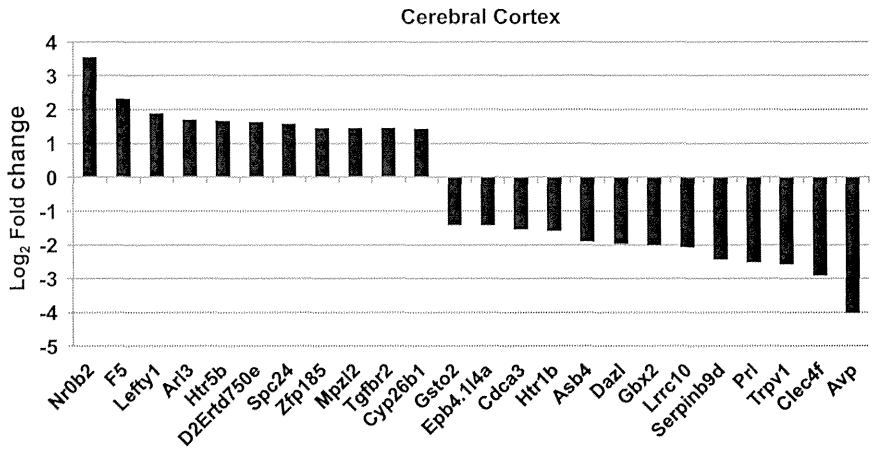

Fig. 3. Microarray analyses in the cerebral cortex. The relative mRNA expression was shown as the log fold-change referring to the control RNA level. Each bar represents a value of pooled RNAs from six mice per group.

Table 3
The relative mRNA expression level of inflammatory markers from dendrimer-treated mice.

Brain area	Dendrimers	*Cox2*	*Ho1*	*qIl1β*	*NfκB*
Olfactory bulb	Control	0.55 ± 0.11	1.40 ± 0.28	1.25 ± 0.82	1.15 ± 0.07
	Low dose	0.55 ± 0.13	1.42 ± 0.23	0.99 ± 0.25	1.35 ± 0.11
	High dose	0.43 ± 0.07	2.00 ± 0.76	1.12 ± 0.41	1.30 ± 0.08
Hippocampus	Control	1.01 ± 0.27	1.02 ± 0.90	0.64 ± 0.29	0.95 ± 0.16
	Low dose	0.87 ± 0.15	0.97 ± 0.11	0.38 ± 0.13	0.78 ± 0.13
	High dose	1.04 ± 0.23	1.24 ± 0.09	0.78 ± 0.28	0.96 ± 0.15
Cerebral cortex	Control	1.69 ± 1.08	1.08 ± 0.07	1.44 ± 0.62	1.05 ± 0.17
	Low dose	2.03 ± 0.85	1.13 ± 0.24	1.24 ± 0.36	1.03 ± 0.10
	High dose	1.58 ± 0.61	1.14 ± 0.14	1.15 ± 0.21	0.95 ± 0.15

Data are normalized for *Rn18s* mRNA levels and represents the mean ± SE ($n = 5$ from each group).
Abbreviations: cyclooxygenase 2; *Cox2*; heme oxygenase 1; *Ho1*; interleukin-1β; *Il1β*; nuclear factor kappa B; *NfκB*.

4. Discussion

The major findings of the present study were that pluripotent network and TGF-beta receptor signaling related-genes were commonly responsive among specific pathways with less than 0.01 of *P*-value in three brain areas by exposure to PAMAM dendrimers. Moreover, the increased expression level of Bdnf gene in the hippocampus and cerebral cortex of high-dose dendrimer-treated mice was observed. To detect the general toxicity of dendrimers, we examined serum biochemical markers and brain inflammatory biomarkers. The results showed that no remarkable changes were observed in the blood or brain. This was the first *in vivo* study to show that the administration of an acute single high dose of dendrimer causes mild effects on neurological gene expressions in the olfactory bulb, hippocampus and cerebral cortex.

Regarding the treatment of central nervous system diseases, it is important to understand the drug delivery system to the brain and to study the toxicity of drug-carrying dendrimers in the brain. There are many routes of administration to the brain, such as intraparenchymal, intraventricular, and subarachnoid injections. In the present study, we used intranasal instillation, which is relevant to human applications. A recent study showed that dendrimers are able to cross the cell membrane of primary neurons, as detected using confocal imaging, and are also able to diffuse to the CNS tissues after intraparenchymal or intraventricular injections (Albertazzi et al., 2013). The same group also demonstrated that the apoptotic cell death of neurons was induced by 100-nm of G4 PAMAM, but not in brain tissues by a sub-micromolar dose. Moreover, using zebra fish embryos, the developmental toxicity of low-generation G3.5 and G4 PAMAM dendrimers has been demonstrated (Heiden et al., 2007).

Some *in vitro* studies have demonstrated that the exposure of human hepatocellular carcinoma (HepG2) cells and human peripheral blood mononuclear cells (PBMCs) from healthy human volunteers to gold nanoparticles capped with PAMAM or sodium citrate (50 μM) might lead to the disturbance of cells, with cytotoxic effects and DNA damage (Paino et al., 2012).

In this study, a microarray analysis showed the up-regulation of the expression levels of genes related to pluripotent network, serotonin-anxiety pathway, TGF-beta receptor signaling, prostaglandin synthesis-regulation, complement-coagulation cascades, blood coagulation cascade and chemokine-signaling pathway and non-odorant GPCR signaling pathways in brain tissues. A trimethyltin-induced model of hippocampal dentate granule cell death dependent upon TNF receptor signaling were demonstrated elevations of TGFβ accompanied with other TNF related cytokines (Funk et al., 2011). Taken together, these results suggest that an acute dose of dendrimers may at least partly cause neuroinflammation and may affect some behavioral functions. Moreover, in the present study, our microarray results showed that Bdnf expression was up-regulated in the hippocampus. This is consistent with mRNA result. It has been reported that BDNF and its signaling pathway involving Akrt, MAPK and P70S6 K are potential target for environmental chemical-induced neurotoxicity (Fattori et al., 2008). BDNF is a neurotrophin and it affects survival and function of neurons in the central nervous system. The up-regulation of Bdnf expression in the present study may be due to body homeostasis, it is also suggested that BDNF-MAPK pathway may involve cellular proliferation, differentiation and inflammation and apoptosis in molecular mechanism.

Regarding the biodistribution of dendrimers, several studies have suggested that the olfactory nerve pathway should be

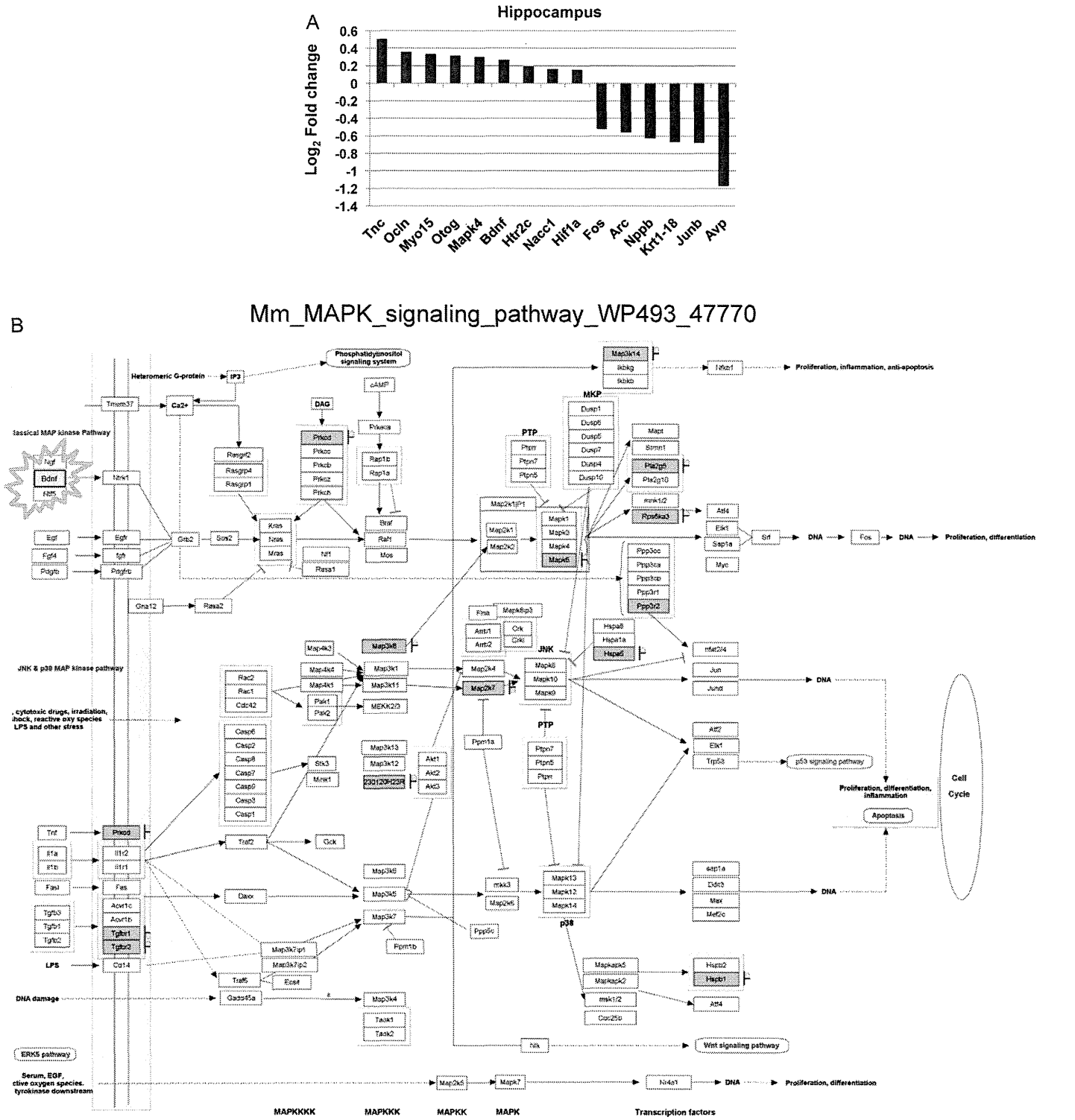

Fig. 4. (A) Microarray analyses in the hippocampus. The relative mRNA expression was shown as the log fold-change referring to the control RNA level. Each bar represents a value of pooled RNAs from six mice per group. (B) Altered gene expression induced by the PAMAM dendrimer exposure were mapped on the BDNF-MAPK signaling pathway in mice of the Wikipathway.

considered as a portal of entry to the central nervous system in humans who are environmentally or occupationally exposed to airborne NPs (Oberdörster et al., 2004; De Lorenzo, 1970; Tjälve et al., 1996). In a landmark study in 1970, De Lorenzo used ultrafine particles to demonstrate that, in squirrel monkeys, intranasally instilled Ag-coated colloidal Au particles (50 nm) translocate anterogradely in the axons of the olfactory nerves to the olfactory bulbs (De Lorenzo, 1970). It has also been shown that manganese (Mn), cadmium (Cd), nickel (Ni), and cobalt (Co) nanomaterials that come into contact with the olfactory epithelium can be transported to the brain *via* olfactory neurons (Tallkvist et al., 1998; Tjälve and Henriksson, 1999; Henriksson and Tjälve, 2000; Persson et al., 2003; Elder et al., 2006). Oberdörster and colleagues demonstrated that the inhalation of ultrafine elemental ^{13}C particles (36 nm)